

**OPTIMIZATION OF FORM AND CONFIGURATION OF
BEADS TO REDUCE THE STRESSES IN A RADIAL FAN**

David Uribe Gallo

UNIVERSIDAD EAFIT
SCHOOL OF ENGINEERING
MECHANICAL ENGINEERING DEPARTMENT
MEDELLIN
2010

OPTIMIZATION OF FORM AND CONFIGURATION OF BEADS TO REDUCE THE STRESSES IN A RADIAL FAN

Student: David Uribe Gallo

Advisors: Prof. Uwe Reinert
Prof. Oscar E. Ruiz

Qualifiers: Prof. Uwe Reinert
Prof. Gerd J. Menken
Prof. Oscar E. Ruiz

Graduation project submitted to the Department of Mechanical Engineering
in partial fulfillment of the requirements for the degree of Bachelor of Science
in Mechanical Engineering at the EAFIT University (Colombia) and
Hochschule Bremen (Germany)

UNIVERSIDAD EAFIT
SCHOOL OF ENGINEERING
MECHANICAL ENGINEERING DEPARTMENT
MEDELLIN
2010

Acknowledgements

To my family, Gladys and Eugenio for supporting me in every step of my formation and giving me the principles that have taken me far.

My most sincere thanks to my advisor Professor Dr. -Eng. Oscar Ruiz for tutoring me in my scientific formation and for setting an example of hard work, discipline and above all honesty.

I will like to thank my advisor Professor Dr. -Eng. Uwe Reinert for teaching me the importance of applying FEM in a practical project and showing me to trust the engineering intuition.

Professor Dr. -Eng. Jens Jensen for his support and trust, from which this adventure wouldn't have taken place.

I would like to thank the people from the CAD/CAM/CAE laboratory, who have shared with me their knowledge and friendship. A special thanks to dipl. Albrecht Eicke for his help and instruction in the Hochschule Bremen.

The faculty members from Universidad EAFIT and Hochschule Bremen for the support on the exchange program between the institutions. This project was partially funded by the Institut für Mechatronische Systementwicklung in Germany and the CAD/CAM/CAE laboratory in Colombia.

Contents

Introduction	xii
Abstract	xiii
1 Literature Review	1
1.1 Radial Fans	1
1.1.1 The Rotor's Components	1
1.2 Stiffening of metallic sheets	2
1.3 Beads	3
1.4 Optimization	6
1.5 Design of experiments	6
2 Loads and Restrictions that Undergoes the Fan's Rotor	9
3 Setting up the Simulation in Patran\Nastran	11
3.1 Creating Patran database files and the nomenclature	11
3.2 Importing the geometry	11
3.3 Creating the mesh	12
3.3.1 Mesh size	12
3.3.2 Patran interface to create the mesh	12
3.4 Creating the Loads and Boundary Conditions	12
3.4.1 Axial restriction of the hub	12
3.4.2 Radial restriction of the hub	13
3.4.3 Centripetal force	15
3.5 Creating the material	15
3.6 Rotor Properties	16
3.7 Creating the Load Case	17
3.8 Solving the Rotor's Rotation	17
3.8.1 Single model	17
3.8.2 Batch run (several model run)	18

4	The Reference Model	20
5	Beads in the Top Ring	22
5.1	Cross section and bead pattern	22
5.2	Variation of the bead pattern	22
5.2.1	Placing the first bead	23
5.2.2	Placing the second bead	23
5.3	Conclusions on placing beads on the top ring	23
6	Beads in the Top Ring	26
6.1	Cross section and bead pattern	26
6.2	Placing of the first bead on the blade	26
6.3	Results after placing the first bead on the blade	26
6.4	Placing of the second bead on the blade	28
6.5	Results after placing the second bead on the blade	28
6.6	Conclusion for the beads on the blades	29
7	Optimization of Bead Patterns Using Design of Experiments	32
7.1	4 level 3 factors experiment design	32
7.1.1	Choosing which tests to run	33
7.1.2	Measuring the goodness of fit from the polynomials	33
7.2	Results using 20 runs design	34
7.2.1	Polynomials describing Maximum Stress Values in the Rotor	35
7.3	Polynomials describing Stress Values in positions 2 and 4	36
7.3.1	Polynomials describing Maximum Deformation Values	36
7.4	Conclusion of Creating Bead Patterns Using Design of Experiments	37
8	Optimizing the Bead's Cross Section	43
8.1	Stress concentration due to small Rad parameter values	44
8.2	Constant $\beta = 90$ degree and $Rad = 3$ varying h and w	45

8.3	Constant $\beta = 60$ degree and $Rad = 5$ varying h and w	46
8.4	Constant $\beta = 90$ degree and $Rad = 5$ varying h and w	46
8.5	Influence of the β angle	47
8.6	Conclusion for Bead Cross Section Optimization	47

Appendices 54

A Matlab script to run multiple .bdf files in series 54

List of Figures

1	Types of Fan Rotors depending of blade geometry. (a) Forward Curved Blades, (b) Radial Blades, (c) Backward Curved Blades.	1
2	Different components of the fan's rotor.	2
2.1	Rotor's top ring.	2
2.2	Rotor's blades	2
2.3	Rotor's bottom ring	2
3	Modifications for a metallic sheet. (a) Original sheet, (b) Topology, (c) Shape, (d) Thickness, (e) Adding elements, (f) Material.	3
4	Four different types of cross sections: (a) box-shaped, (b) round-shaped, (c) v-shaped and (d) trapezoidal.	4
5	figure of a beaded cross section (left) and an unbeaded cross section (right). . .	4
6	3 levels factorial designs with 2 or 3 factors.	7
6.1	3^2 factorial design.	7
6.2	3^3 factorial design.	7
7	Forces that affect the fan's rotor.	9
7.1	Inertial forces due to rotation (F_{rot})	9
7.2	Inertial forces due to gravity (F_g)	9
7.3	Forces due to air pressure on the blades (F_p)	9
8	Forces that affect the fan's rotor.	10
8.1	Axial restriction of the rotor.	10
8.2	Radial restriction of the rotor.	10
9	Changing the import units of a Parasolid model to millimeters.	11
10	Mesh size determination graph	12
11	Patran Elements interface configuration.	13
12	Geometry selection to restrict in axial direction	14
13	Geometry selection to restrict in radial direction	14
14	Input properties menu from the Properties tab.	16
15	Input menu for the Load Cases tab.	17

16	Subcase select menu for the analysis tab.	18
17	Matlab batch run script menu.	19
18	Stress measuring positions of the reference model.	20
19	Von Mises stress distribution of the blade in the reference model.	21
20	Cross section of round bead.	22
21	Bead pattern of top ring beads.	22
22	Placing of the first bead in the top ring.	23
	22.1 Bead pattern parameter for the first bead.	23
	22.2 Simulations to place the first bead.	23
23	Placing of the second bead in the top ring.	24
	23.1 Bead pattern parameter for the second bead.	24
	23.2 Simulations to place the second bead.	24
24	Von Mises stress distribution on the top ring after being beaded.	25
25	Parameters and measuring positions for placing the first bead on the blade. . . .	27
	25.1 Parameters of the first bead pattern on the blade.	27
	25.2 Measuring positions of the first bead on the blade model.	27
26	Von Mises stress distribution in the blade after adding one Bead.	27
27	Von Mises stress distribution in the top ring after adding one bead.	28
28	Parameters and measuring positions for placing the second bead on the blade. .	29
	28.1 Parameters of the second bead pattern on the blade	29
	28.2 Measuring positions of the second bead on the blade model.	29
29	Von Mises stress distribution in the blade after adding two beads.	30
30	Von Mises stress distribution in the top ring after adding two beads.	30
31	Sphere diagram of 64 simulations to find the best bead pattern for the one-beaded model.	31
32	Sphere diagram of 64 simulations to find the best bead pattern for the two-beaded model.	31
33	Different design of experiments in a 4^3 space according to Koukouvinos	34
	33.1 20 runs design of experiments.	34

33.2	36 runs design of experiments.	34
33.3	48 runs design of experiments.	34
33.4	64 runs (Full Factorial design of experiments).	34
34	Measuring the goodness of fit for different polynomials from measurement data in the fan's rotor.	35
34.1	R^2 values of the polynomials that fit the Stress values in the middle of the blade.	35
34.2	R^2 values of the polynomials that fit the nodal displacement data.	35
34.3	R^2 values of the polynomials that fit the maximum stress values.	35
34.4	R^2 values of the polynomials that fit the Stress values in the top of the bead.	35
35	Linear, Quadratic and Cubic approximations of the σ_r function.	37
35.1	Linear polynomial approximation of σ_r with 20 runs.	37
35.2	Quadratic polynomial approximation of σ_r with 20 runs.	37
35.3	Cubic polynomial approximation of σ_r with 20 runs.	37
35.4	Cubic polynomial approximation of σ_r using 64 runs (full factorial design).	37
36	Linear, Quadratic and Cubic approximations of the σ_2 function.	38
36.1	Linear polynomial approximation of σ_2 with 20 runs.	38
36.2	Quadratic polynomial approximation of σ_2 with 20 runs.	38
36.3	Cubic polynomial approximation of σ_2 with 20 runs.	38
36.4	Cubic polynomial approximation of σ_2 using 64 runs (full factorial design).	38
37	Linear, Quadratic and Cubic approximations of the σ_4 function.	39
37.1	Linear polynomial approximation of σ_4 with 20 runs.	39
37.2	Quadratic polynomial approximation of σ_4 with 20 runs.	39
37.3	Cubic polynomial approximation of σ_4 with 20 runs.	39
37.4	Cubic polynomial approximation of σ_4 using 64 runs (full factorial design).	39
38	Linear, Quadratic and Cubic approximations of the d_r function.	40
38.1	Linear polynomial approximation of d_r with 20 runs.	40
38.2	Quadratic polynomial approximation of d_r with 20 runs.	40
38.3	Cubic polynomial approximation of d_r with 20 runs.	40

38.4	Cubic polynomial approximation of d_r using 64 runs (full factorial design).	40
39	Optimized bead beaded blade with nodal displacement colormap.	40
40	Unbead blade with nodal displacement colormap.	41
41	Back view of the unbeaded blade with Von Mises colormap.	41
42	Back view of the optimized bead beaded blade with Von Mises colormap.	42
43	Global parameters of a bead's cross section.	43
44	Top ring generatrix with varying β angle.	44
44.1	Generatrix of $\beta = 45$ model.	44
44.2	Generatrix of $\beta = 60$ model.	44
44.3	Generatrix of $\beta = 75$ model.	44
44.4	Generatrix of $\beta = 90$ model.	44
45	Model with parameter $Rad = 3$ mm	45
46	Model with parameter $Rad = 5$ mm	45
47	Surfaces describing the Stress and Nodal Displacement behavior of $\beta = 90$ degree and $Rad = 3$ models.	46
47.1	Maximum nodal displacement of the 90 degree, $Rad = 3$ models.	46
47.2	Stress values at highest displacement point of the 90 degree, $Rad = 3$ models.	46
47.3	Maximum Stress of the 90 degree, $Rad = 3$ models.	46
48	Surfaces describing the Stress and Nodal Displacement behavior of $\beta = 60$ degree and $Rad = 5$ models.	47
48.1	Maximum nodal displacement of the 60 degree, $Rad = 5$ models.	47
48.2	Stress values at highest displacement point of the 60 degree, $Rad = 5$ models.	47
48.3	Maximum Stress of the 60 degree, $Rad = 5$ models.	47
49	Surfaces describing the Stress and Nodal Displacement behavior of $\beta = 90$ degree and $Rad = 5$ models.	48
49.1	Maximum nodal displacement of the 90 degree, $Rad = 5$ models.	48
49.2	Stress values at highest displacement point of the 90 degree, $Rad = 5$ models.	48
49.3	Maximum Stress of the 90 degree, $Rad = 5$ models.	48
50	Influence of the β angle.	49

50.1	Influence of β angle against maximum displacement	49
50.2	Influence of β angle against stress variation	49
51	Two views comparing the nodal displacement between the 60 and 90 degrees models	49
51.1	Displacement comparison of 60 (red) and 90 (blue) degrees models (lateral view)	49
51.2	Displacement comparison of 60 and 90 degrees models (isometric view) . .	49
52	Displacement distribution colormap.	49
53	Von Mises stress distribution colormap.	50
54	Two renders of the cross sections of the optimized beads.	50
54.1	Final cross section of the blade.	50
54.2	Final cross section of the top ring.	50

List of Tables

1	Von Mises stress values of the reference model at given measuring points (MPa).	20
2	Von Mises stress values after placing 2 beads on the top ring (MPa).	24
3	Von Mises stress values after placing 1 bead on the blade.	28
4	Von Mises stress values after placing 2 beads on the blade.	29
5	Predicted minimum values for the σ_r function and the bead pattern parameters.	36
6	Predicted minimum values for the σ_2 function and the bead pattern parameters.	36
7	Predicted minimum values for the σ_4 function and the bead pattern parameters.	36
8	Predicted minimum values for the d_r function and the bead pattern parameters.	37

Symbols

b_i	Limits of the constraint function
B_{L1}, B_{L2}, B_{L3}	Parameters of the second bead pattern in the blade
B_{R1}, B_{R2}, B_{R3}	Parameters of the first bead pattern in the blade
d_r	Nodal displacement function of the rotor
$f_0(x)$	Objective function of an optimization problem
$f_i(x)$	Constraint functions of an optimization problem
h	Bead depth
h_s	Height of the bead arm
H_{SR1}, H_{SR2}	Parameters of the first and second bead patterns in the top ring
I	Second moment of area
m	Number of restrictions
$max()$	Maximization function
$min()$	Minimization function
n	Degree of a polynomial
R^2	Coefficient of determination
R_{st}	Stamping radius of a round bead
R_z	Forming Radius of a round bead
S_a	Response surface
t	Sheet metal thickness
w	Width of a bead
β	Forming angle of a trapezoidal bead
η	Mechanical efficiency of a fan
σ_i	Von Mises stress function of the rotor on the point i
σ_r	Maximum Von Mises stress function of the rotor
ω	Angular or rotational speed

Introduction

Radial fans are light structures that have the task of displacing the most amount of air possible. It is of big interest to operate such devices at the maximum angular speed possible to increase the airflow. Most fans are restricted to a maximum angular speed in order to operate without it auto-destructing. In many applications the use of a second fan is needed because a single fan won't provide enough airflow.

The improvement of the fans will spare the user in many cases of wasting design space placing a second fan, reducing operational costs and add efficiency in some processes that require concentrated airflow.

The biggest challenge of building light structures is obtaining the necessary structural strength for it to perform safely. Due to the nature of radial fans, the most destructive force that they undergo is the centripetal force. This force exhibits a quadratic growth as the angular speed increases. This force will increase as well by adding any material to the rotor.

The problem of strengthening metallic sheet is generally a complex task that involves FEA solutions. This work presents two methods developed to calculate the correct dimensioning and positioning of beads in metallic sheet to reduce the stresses that a fan rotor experiences. These methods heavily rely in CAD software and not CAE as modern methods do. The most important features that are discussed are i) the manufacturability of the bead geometries and ii) the effectiveness of the bead geometries to decrease the stress and deformation values in the fan's rotor. The methods are not restricted to this project and can be further used for other mechanical parts.

In chapter 1 a literature review introduces all the necessary concepts and state of the art necessary to understand fans and strengthening of metallic sheets. Chapter 2 explains the different loads that the fan undergoes in real life and the assumptions made for the FE model. Chapter 3 explains the correct setup in the software Patran to simulate the fan model. Later chapter 4 explains the stresses and the deformations of the reference model.

Chapter 5 and 6 explain the new methods to add beads in the metallic sheet. Finally chapter 7 and 8 use optimization techniques to find optimal bead shapes (patterns) and cross sections.

Abstract

One of the major problems associated to thin metallic structures is its lack of structural stiffness and the complexity to reinforce such structures without adding weight. One common technique used to increase the structural stiffness is called beading. The use of these stiffeners usually relies on pre-established bead-patterns or computer-generated complicated geometries that sometimes are not possible to manufacture or concur on high manufacturing prices.

This thesis will explain a robust approach to find bead geometries that: (i) are possible to manufacture and (ii) reduce considerably the stress values and deformation of a mechanical part. The most important characteristic of the work is to establish methodologies that don't require a very high expertise from the user on the geometric calculations that current authors have established, but that have a high effectiveness as well.

The procedure for the work consists of an initial extensive literature review on light-weight structures, mechanization and design of Beadings, radial fans and optimization techniques. Using the geometry of a radial fan as a case study, the methodologies developed from the investigation will be tested to find the effectiveness of them. The tests from the radial ventilator will be carried on using valid FEM simulations to avoid high costs. All the results will be tabulated and presented. The appropriate conclusions will be done

1 Literature Review

1.1 Radial Fans

There are several types of radial fans which are normally classified depending on their uses. Overall, this type of fan can be classified as well by its blade geometry against its sense of rotation. Figure 1.1 shows a sketch of the top view of the rotors of 3 different fan configurations. From [1], it is known that the mechanical efficiencies of the different fans are as in equation 1.

$$\eta_{(b)} < \eta_{(a)} < \eta_{(c)} \quad (1)$$

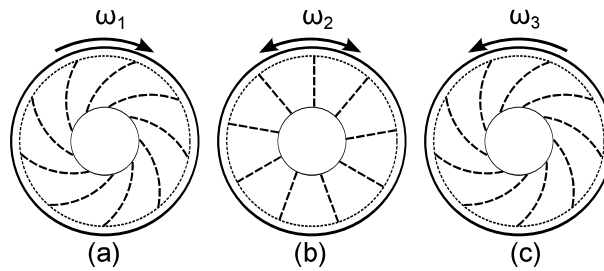


Figure 1: Types of Fan Rotors depending of blade geometry. (a) Forward Curved Blades, (b) Radial Blades, (c) Backward Curved Blades.

This work discusses the type (c) fan. This type of fan is known for its high efficiency, low pressure, and high volumetric flow. It can handle particles in the air and its design relies mainly on empirical formulas [2].

1.1.1 The Rotor's Components

The rotor has 3 different components. i) A top ring, ii) blades and iii) a bottom ring. Empirical data shows that rotors fail due to the blade components. The bottom ring and the top ring are created by a generatrix, that runs along the y-axis in the CAD program. Fan manufacturers commonly reference their fans by the top ring diameter followed by other specifications. This project evaluates a “630” reference from the firma mdexx. The results can be later compared with the fans from firms such as ebm-papst¹, Kice industries² and others that offer similar references.

¹http://www.ebmpapst.com/en/products/centrifugal-fans/backward-curved/backward_curved.php

²<http://www.kice.com/Product-CentrifugalFans.html>

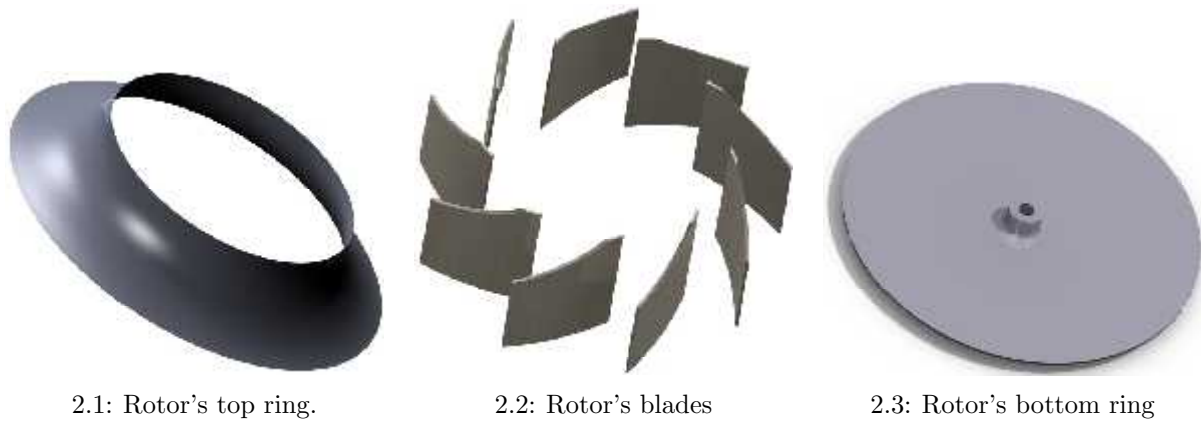


Figure 2: Different components of the fan's rotor.

1.2 Stiffening of metallic sheets

Often the functional design restrictions of thin-walled mechanical parts restrict the compliance of material resistance, vibrations and deformation. For this reason, the metallic sheet must be slightly modified in such a way that the function is not greatly affected, and the mechanical part can still perform safely.

Emmrich [3] speaks of 4 different types of possible modifications, while Klein [4] describes 3 and Schwarz [5] speaks mainly about 2. The main ideas of the authors can be condensed in 5 categories:

- i. Topological: Having a defined workspace or restricted space, it's the ability to arrange the metallic sheet's material in different configurations. Moreover, it can be from simple perforations to complicated contours.
- ii. Shape or Form: The metallic sheet form is no longer restricted to a space. This means it can be freely deformed to take advantage of certain shapes that give metallic sheets special characteristics.
- iii. Thickness variation: This technique is not widely use on metallic sheets, although it is very common on other materials such as composites or plastic laminates.
- iv. Adding Stiffening Elements: The most common elements are Ribs, which are itself a structure of its own, and then welded to the metallic sheet.
- v. Material: The range of modifications that can be done with the material can be sometimes overwhelming. The two governing factors to modify the material are costs and ease to mechanize. This is a very strong topic today for composite materials.

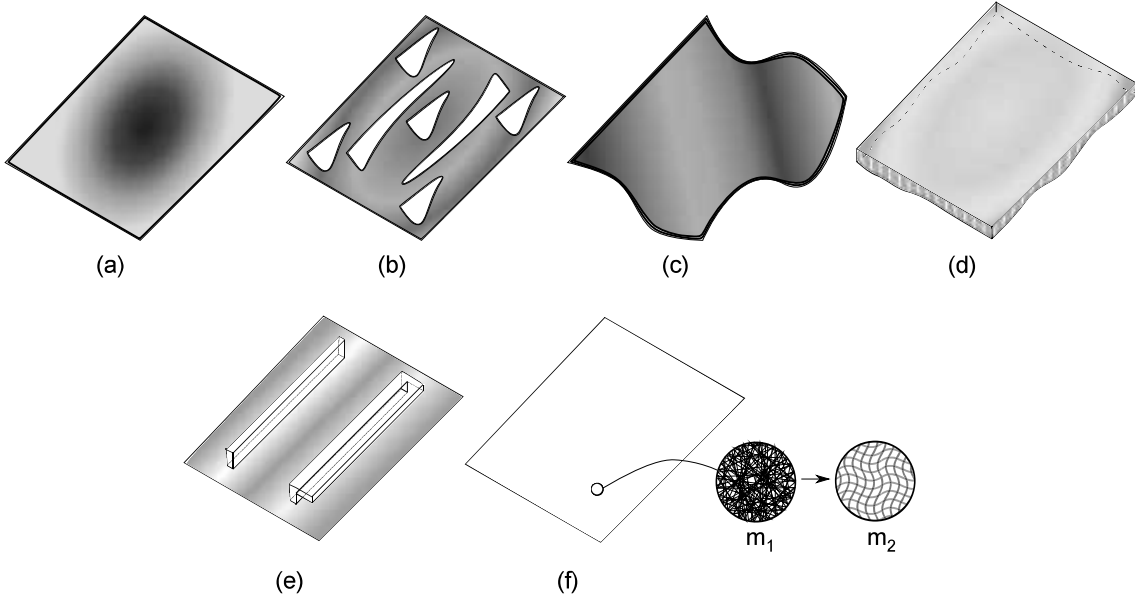


Figure 3: Modifications for a metallic sheet. (a) Original sheet, (b) Topology, (c) Shape, (d) Thickness, (e) Adding elements, (f) Material.

The most common approach to modify the metallic sheet of light-weight structures is called fully-stressed design. This method chooses a combination of the possible modifications in order to achieve an equal stress distribution in the metal sheet. This method is the most common approach used by several authors to design light-weight structures [6]. This was further developed for sheet metal by [5], [3] and [7]. The firms Altair, Tosca and Sachs-Engineering have created their products on this principle as well.

1.3 Beads

The definition from Bead is “A groove on a metallic sheet, being the groove’s depth significantly smaller than its length.” The width of the bead has aroused some questions since some authors defend the use of large width values. Other authors defend the use of widths slightly larger than the depth. There are two global aspects that define a bead: cross section and bead pattern.

There are four types of cross sections (see figure 4). The way a bead works is by displacing material from the neutral fibers. Given this displacement, a term in the second moment of area appears. This term grows in a quadratic way as the material is further from the neutral fibers. Therefore the depth of the bead is an important factor. Figure 5 shows a schematic comparison of a beaded and a flat cross section with similar widths. Using the parameters from this figure, it is proven in equation 2 that the second moment of area is significantly larger in a beaded cross sections [5].

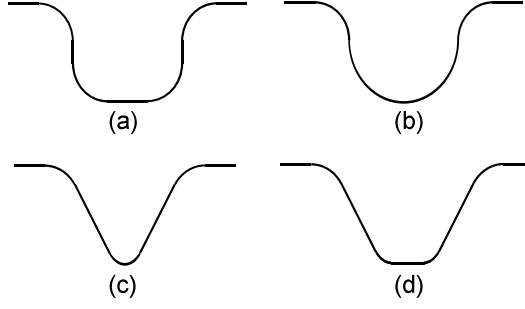


Figure 4: Four different types of cross sections: (a) box-shaped, (b) round-shaped, (c) v-shaped and (d) trapezoidal.

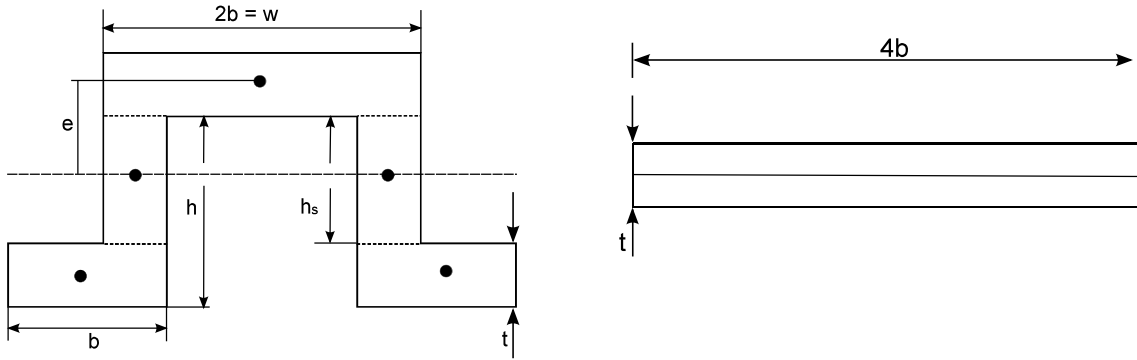


Figure 5: figure of a beaded cross section (left) and an unbeaded cross section (right).

$$\begin{aligned}
 I_{beaded} &= 2 \left(\frac{th_s^3}{12} \right) + 2 \left(\frac{bt^3}{12} + e^2bt \right) + \left(\frac{2bt^3}{12} + e^22bt \right) \\
 I_{unbeaded} &= \frac{4bt^3}{12} \\
 I_{beaded} &\gg I_{unbeaded}
 \end{aligned} \tag{2}$$

The first studies of beads was finding manufacturable geometries for the automotive industry. Oehler [8] suggested the use of only round-shaped beads. An important contribution from this work was the restriction that no axis should exist in the plate that would not collide with a bead. Kiensle [9] studied the effect of the bead depth. He also found that box shaped beads had the best stiffening effects. A 10% correction factor was proposed when calculating beads.

In 1971, Oehler and Draeger [10] measured the buckling effect of a circular plate with a singular bead. They would find that the angle at which the bead was placed would determine its effectiveness. It was also shown that a bad placed bead would decrease the stiffness from the original plate (meaning that no beading is better as “bad” beading).

The next year Oehler and Weber would publish a catalog of bead patterns for specific load cases [11]. In this work, the first non-straight beads were created. They were all created from

empirical data. This bead patterns would be then used in the industry for several years.

The first use of numerical methods to calculate beads was in 1984 by Wildmann [12]. It was found that the predominant factor in beads was its pattern and not the cross section. He compared the numerical simulations and real models and concluded that the simulations correctly described the phenomenon. A correction factor between 10% and 15% was proposed.

Klein would show that bead patterns should follow the principal stress vector direction [13]. The cross section for this pattern was done by setting a high-temperature to the bead pattern. Afterwards the iso-temperature curves around the pattern would be heighten respecting it's temperature value. This led sometimes to non-manufacturable geometries.

Herrmann proved that the use of small deformation models was enough to simulate beaded plates in the elastic deformation interval (saving time on costly large deformations models) [14]. In this work, a circular pattern was set in top of the plate, and after each iteration the pattern was deformed by intuition.

In 2002 Schwarz [7] would recreate the work by Oehler in 1972 and create pre-established bead patterns. His work would be called "Sickenatlas", or bead-atlas. He used the software Optistruct from the firma Altair Hyperworks³. Optistruct uses form vectors in each node. These vectors are each a variable from a function. The goal from Optistruct is then to minimize this function given the variables. When the program finds the function's minimums, it gives the user a picture that must be interpreted into geometric forms. The Sickenatlas was then Schwarz interpretation of the results given by Optistruct. One of the most important findings from this work was a revision of the FEM against real models with many load cases. Just like in [12], it was probed that the FEM approach is valid.

In his doctorate dissertation [5], Schwarz would further improve his method from the Sickenatlas and create an interpreter for the program Optistruct.

Emmrich in his doctorate dissertation [3] would develop a method to find bead patterns without the "optimal" characteristic that other authors were looking after. This method was further developed in a module for Tosca Structure ⁴ called Tosca.bead.

In the past years, the trend in beading investigation is in terms of manufacturability. Most projects work with the Tosca software or Optistruct. An example for this is the work by Kroenauer et al. [15].

³<http://www.altairhyperworks.com/Product,19,OptiStruct.aspx>

⁴<http://www.fe-design.de/toscabead.html>

1.4 Optimization

An optimization problem [16] has the following statement as in equation 3. Where the vector $x = (x_1, \dots, x_n)$: is the optimization variable, the function $f_0(x) : R^n \rightarrow R$ is the objective function, the functions $f_i(x) : R^n \rightarrow R$, $i = 1, \dots, m$, are the (inequality) constraint functions, and the constants b_1, \dots, b_m are the limits, or bounds, for the constraints. A vector x^* is called optimal, or a solution of equation 3 if it has the smallest objective value among all vectors that satisfy the constraints: for any z with $f_1(z) \leq b_1, \dots, f_m(z) \leq b_m$, we have $f_0(z) \geq f_0(x^*)$.

$$\begin{aligned} & \min (f_o(x)) \\ & \text{subject to } f_i(x) \leq b_i \end{aligned} \tag{3}$$

There are several mathematical methods to solve the minimization problem. This project focused on the use of response surfaces. This method finds a surface (hypersurface given the case) $S_a(x)$ with at least C^1 continuity that accurately describes the objective function. That means that $S_a(x) \approx f_0(x)$. Since S_a is once differentiable, it is possible to find a global minimum of $S_a(x)$. This will then be the answer for the optimization problem.

The most common Response Surfaces have the form described in equation 4. Here $a_i : i = 1, 2, \dots, n + 1$ are the polynomial constants, and are the values that give the approximation to the objective function. The determination of these constants is the biggest challenge for this optimization approach. Inherent from this method, there is an error e . This error has two components: the first one is a natural error that has any measurement in an experiment (hysteresis, human error, etc.) and a second one due to surface fitting from the data collected (numerical error). These are too polynomials of degree n , and are usually first, second and third degree polynomials. The degree of the polynomial is chosen depending of the experiment. Sometimes this type of approach to solve the minimization problem may not be suitable.

$$S_a^n(x) = a_1x^0 + a_2x^1 + \dots + a_{i+1}x^i + \dots + a_{n+1}x^n + e \tag{4}$$

1.5 Design of experiments

One of the most important tasks of Design of Experiments is creating methods to determine the values of the constants described in section 1.4 with accuracy and less data dependence. Depending on the degree and number of variables of the approximation polynomial, different methods are used.

Concerning Design of Experiments, the variables x_i are referred as “factors”. These factors are

then varied a certain amount of times, called “levels”. To better illustrate this, figure 6.1 shows a 2 factors, 3 levels design. The gray square represents the design space. Every black point is a measurement taken from the experiment. This method is further explained in [17].

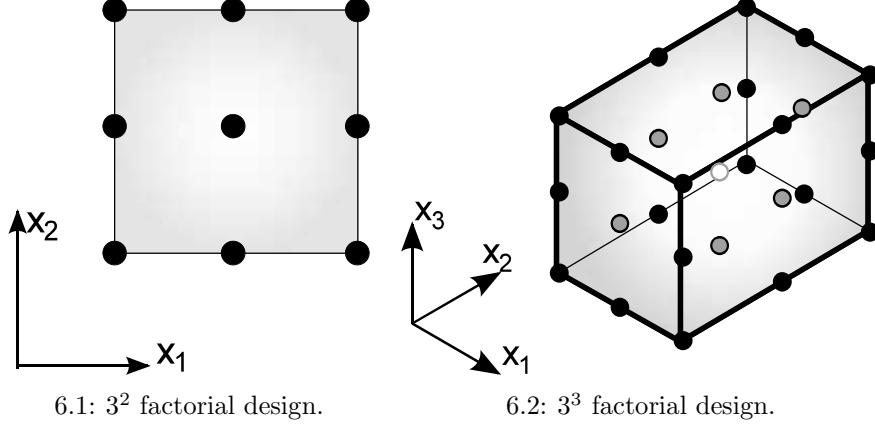


Figure 6: 3 levels factorial designs with 2 or 3 factors.

In order to reduce the amount of experiments required to find accurate ai values, there are two common methods, the Box-Wilson Central Composite Design and the Box-Behnken Design. These experiment designs are further explained in [18].

After choosing the experiments that are going to take place (x_i), there is a system of linear equations of dimension $m \times (n + 1)$, where $m \geq (n + 1)$.

$$\begin{aligned}
 \begin{bmatrix} y_1 \\ y_2 \\ \vdots \\ y_m \end{bmatrix} &= \begin{bmatrix} a_1 x_{1,1}^n & a_2 x_{1,2}^{n-1} & \cdots & a_{n+1} x_{1,n}^0 \\ a_1 x_{2,1}^n & a_2 x_{2,2}^{n-1} & \cdots & a_{n+1} x_{2,n}^0 \\ \vdots & \vdots & \ddots & \vdots \\ a_1 x_{m,1}^n & a_2 x_{m,2}^{n-1} & \cdots & a_{n+1} x_{m,n}^0 \end{bmatrix} \\
 \begin{bmatrix} y_1 \\ y_2 \\ \vdots \\ y_m \end{bmatrix} &= \begin{bmatrix} x_{1,1}^n & x_{1,2}^{n-1} & \cdots & x_{1,n}^0 \\ x_{2,1}^n & x_{2,2}^{n-1} & \cdots & x_{2,n}^0 \\ \vdots & \vdots & \ddots & \vdots \\ x_{m,1}^n & x_{m,2}^{n-1} & \cdots & x_{m,n}^0 \end{bmatrix} \begin{bmatrix} a_1 \\ a_2 \\ \vdots \\ a_{n+1} \end{bmatrix} \\
 y &= Xa
 \end{aligned} \tag{5}$$

Here y_i is the i th result from the experiment that describes the i th equation. Since X from equation 5 may not be squared, the solution for a is found using the Moore-Penrose pseudoinverse. This solution is the same as a least square regression. Equation 6 is the pseudoinverse equation.

$$a = (X^T X)^{-1} X^T y \tag{6}$$

2 Loads and Restrictions that Undergoes the Fan's Rotor

The first step towards determining the appropriate finite element model is to know the interactions of the mechanical part with its surroundings. Basically 3 types of forces affect the rotor: centripetal (F_{rot} , figure 7.1), gravitational (F_g , figure 7.2), and drag (F_p , figure 7.3).

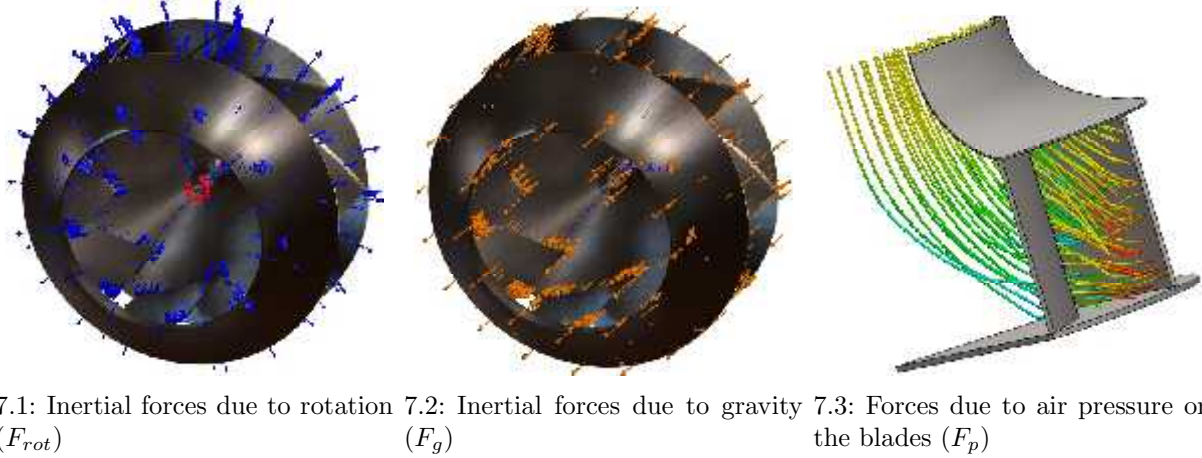
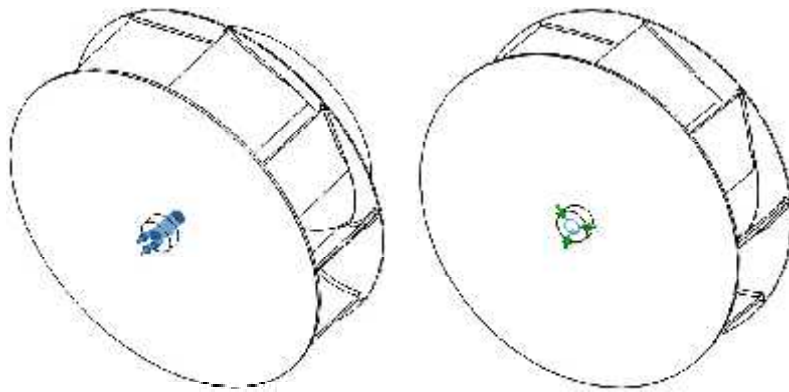


Figure 7: Forces that affect the fan's rotor.

Due to the light-weight design, low air pressure and high rotational speeds, it is accurate to say that $F_{rot} \gg F_g, F_p$. For this reason, the only force taken into account in the simulations is the centripetal one. The second assumption is that the rotor has its highest stress value when it is running in its operation point. This means that it is running at a constant angular speed: $\omega = 25\text{Hz}$.

With these assumptions, the load case can be simplified enough to create a static approximation. Therefore the shaft-hub interaction is simulated so that the draft and gravitational forces have no effect on it. This means that the model is restricted just enough to have a static-determined Finite Element Analysis. These restrictions can be seen on figure 8.1 and figure 8.2. There are combinations of restrictions that would give similar results. This one was chosen in order to compare historical results from previous groups that did work on the same rotor.



8.1: Axial restriction of the rotor. 8.2: Radial restriction of the rotor.

Figure 8: Forces that affect the fan's rotor.

3 Setting up the Simulation in Patran\Nastran

The software Patran 2008 r1 from the firm MSC Software was used as pre\post processor. As solver, the software Nastran 2008 r3b from the same firm was used. In order to run several files in the solver, a Matlab script was created (append A). The following sub-sections explain the correct configuration for Patran/Nastran in order to simulate the fan's rotor.

3.1 Creating Patran database files and the nomenclature

After opening the Patran program, the first step is creating a new database file (.db extension). The nomenclature used in this project was key to make the results easier to classify later. It was as follows: (sub-project-name)-(reference-number)-(special-annotations).db. An example would be: double-bead-topring_001_angle-60.db.

3.2 Importing the geometry

The files used for this project were from the Parasolid kernel, with the .xt extension. They were created using SolidWorks 2009 r1. When clicking on the File→Import icon, the import dialog pops up. After finding the desired .xt file, the dimensional units in which Patran imports the file must be changed (the default units are inches). On figure 9 the 3 necessary steps to change the units is shown. The blue square indicates the icon that needs to be clicked.

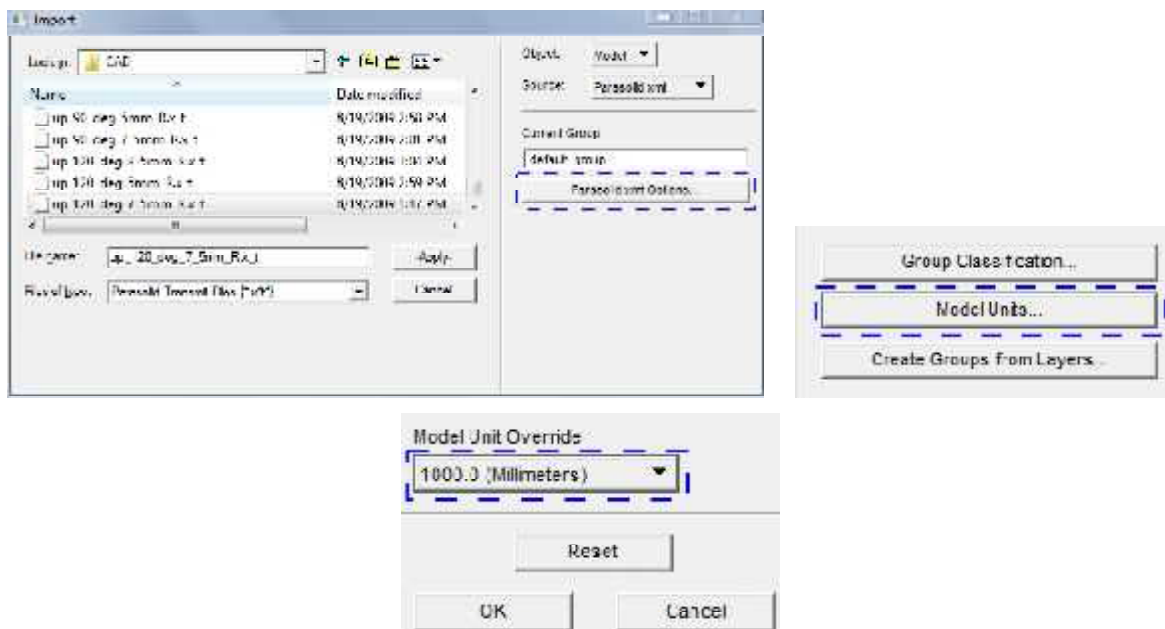


Figure 9: Changing the import units of a Parasolid model to millimeters.

3.3 Creating the mesh

3.3.1 Mesh size

Patran is able to create curvature sensible meshes. The only parameter necessary to vary is the Global edge length. To measure a good mesh size, this parameter was lowered (a finer mesh) until the Von Mises Stress value was constant. Using the graph in figure 10, it was determined that the best Global Edge Length is 6 mm.

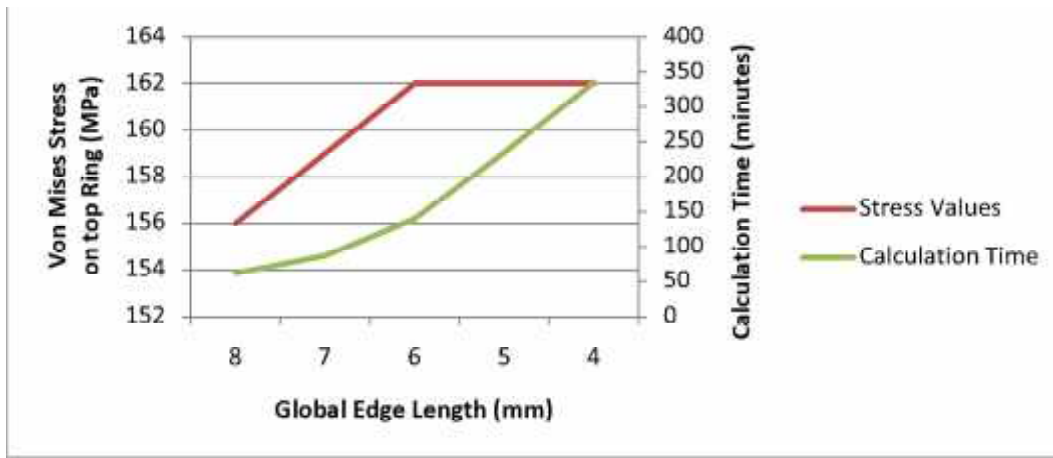


Figure 10: Mesh size determination graph

3.3.2 Patran interface to create the mesh

When clicking on the “Elements” tab on the user interface, a menu will appear on the right side of the screen. The inputs required on this menu are shown on figure 11. Notice that the value on the “Global Edge Length” was set to 6, as calculated on section 3.3.1.

3.4 Creating the Loads and Boundary Conditions

From the description in section 2, there are 3 different parameters as input under the tab “Loads/BCs” in the Patran interface.

3.4.1 Axial restriction of the hub

When the “Loads BCs” tab is clicked, a menu appears on the right side of the screen. The correct configuration for the menu is:

1. Action: Create

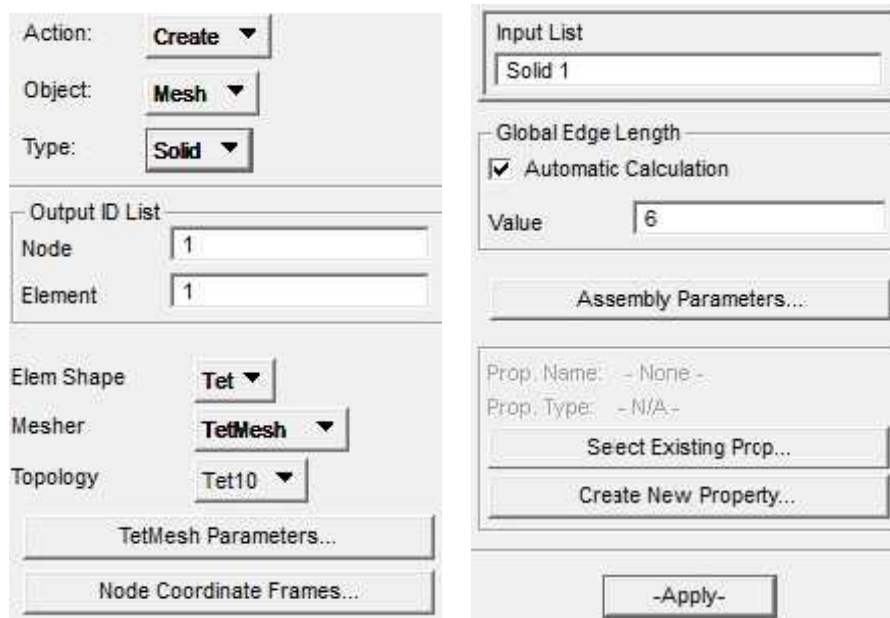


Figure 11: Patran Elements interface configuration.

2. Object: Displacement
3. Type: Nodal
4. Option Standard
5. New Set Name: hub_y_sense (note :this is written by the user)

Afterwards, click on the “Input Data” icon and write: Translations $\langle, 0, \rangle$. Then click “ok”. Finally click on the “Select Application Region.” icon. In order to be able to select surfaces, click on the small icon enclosed by the small red rectangle on figure 12. Then click the inner surface of the hub (the one shown on figure 8.1). A number will appear on the “Select Geometry Entities” with the nomenclature “Solid 1.xx”, where “xx” is the surface number. Click on add. To end the procedure, click on ok, and then on apply. The Load will be saved in Patran’s database.

3.4.2 Radial restriction of the hub

When the “LoadsBCs” tab is clicked, a menu appears on the right side of the screen. The correct configuration for the menu is:

1. Action: Create
2. Object: Displacement

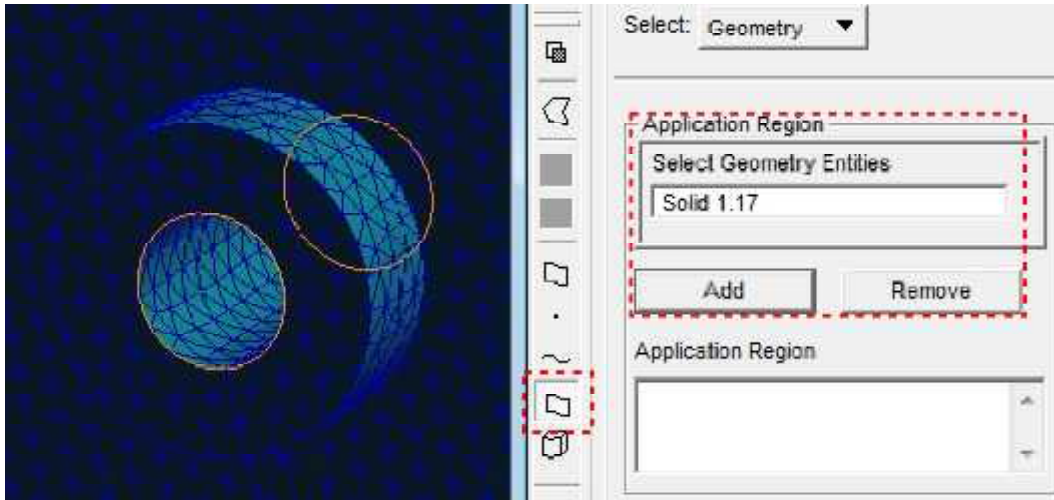


Figure 12: Geometry selection to restrict in axial direction

3. Type: Nodal
4. Option Standard
5. New Set Name: hub_xz_sense (note :this is written by the user)

Afterwards, click on the “Input Data” icon and write: Translations $\langle 0, , 0 \rangle$. Then click “ok”. Finally click on the “Select Application Region.” icon. In figure 13 the region application menu is shown. Click the edge selection tool, and then click on the lowest curve in the hub as in figure 8.2. Finish the procedure as done with the axial restriction in the previous section.

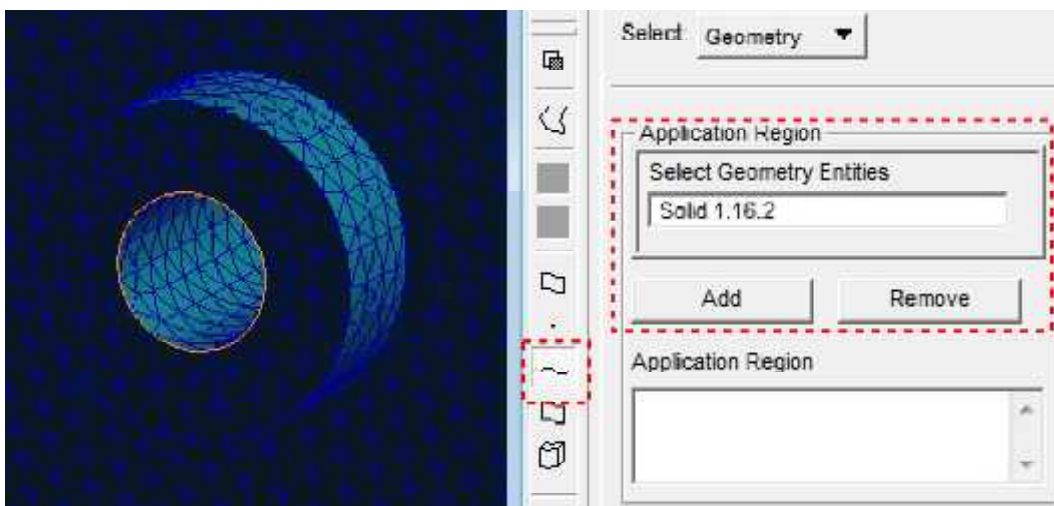


Figure 13: Geometry selection to restrict in radial direction

3.4.3 Centripetal force

To set up the centripetal forces exerted by the rotational speed, change the menu settings for the “Loads/BCs” tab as follows:

1. Action: Create
2. Object: Inertial Load
3. Type: Element Uniform
4. Option Standard
5. New Set Name: rotational_speed (note :this is written by the user)

When this information is in the menu spaces, click on the ”Input Data” icon. The input for this menu is:

1. Trans Accel: (note: no input)
2. Rot Velocity: <,25,>
3. Rot Accel : (note: no input)

Finally click “ok” and then “apply”. The rotational speed information will be saved in Patran’s database.

3.5 Creating the material

The material used for this project has a Poisson Ratio of 0.3, an Elastic Modulus of 210 MPa a density of 7850 kg per cubic meter and a Yield Strength of 235 MPa. After clicking the Material tab, input the following information:

1. Action: Create
2. Object: Isotropic
3. Method: Manual Input
4. Material Name: steel

Click on the “Input Properties” icon and enter the following information:

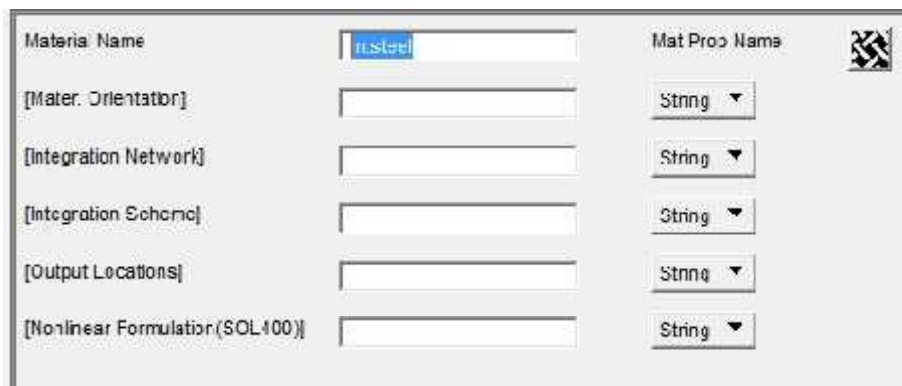
1. Constitutive Model: Linear Elastic
2. Elastic Modulus: 210000
3. Poisson Ratio: 0.3
4. Density: 0.00000785

To finish, click on ok and then the “apply” button. This will save the material “steel” on the database.

3.6 Rotor Properties

To assign the material properties to the rotor, click on the “Properties” tab. Then input the following information:

1. Action: Create
2. Object: 3D
3. Type: Solid
4. Property Set Name: rotor_properties




Material Name	<input type="text" value="steel"/>	Mat Prop Name	
[Material Orientation]	<input type="text"/>	String	▼
[Integration Network]	<input type="text"/>	String	▼
[Integration Scheme]	<input type="text"/>	String	▼
[Output Locations]	<input type="text"/>	String	▼
[Nonlinear Formulation (SOL100)]	<input type="text"/>	String	▼

Figure 14: Input properties menu from the Properties tab.

Click Input Properties. Input the information in figure 14. Afterwards click on “ok” and finally “apply”. Now Patran recognizes that the rotor is made out of “steel”.

3.7 Creating the Load Case

Now it's necessary to create a Load Case. Click on the “Load Ca” tab. Input the following information:

1. Load Case Name: rotation
2. Type: Static

The screenshot shows a software interface for selecting loads and boundary conditions. It features two list boxes at the top: 'Select individual Loads/BCs' on the left and 'Select Loads/BCs from Existing Load Cases' on the right. Below these is a button labeled 'Additional Loads/BCs Controls'. At the bottom, there is a section titled 'Assigned Loads/BCs' which includes a 'Don't By Priority' button and a 'Load/BC Type' dropdown menu currently set to 'Displacement'. Below this is a table with the following data:

	Type	Scale factor	Priority
hub_XZ_sensor	Displacement	1	Add
hub_y_sensor	Displacement	1	Add
rotational_speed	inertial Load	1	Add

Figure 15: Input menu for the Load Cases tab.

Click in the “Input Data” icon. The menu on figure 15 will pop up. Under “Select Individual Loads/BCs” all the previously created loads are show. Click on each load. In a menu under (Assigned Loads/BCs) each load will appear as it is clicked. Finish by clicking “ok” and then “apply”. Now Patran saves in its database the simulation environment necessary to emulate the rotor’s rotation.

3.8 Solving the Rotor’s Rotation

To solve the finite elements problem, click on the “Analysis” tab. There are two possibilities, either do a batch run (simulate many models at a time) or run a single model.

3.8.1 Single model

To run a single model, set the following parameters:

1. Action: Analyze

2. Object: Entire Model
3. Method: Full Run

The Job Name is the same as the database name. Click on the “Subcase Select” icon. The menu on figure 16 will pop up. On the upper list, click on the “rotation” line. The “rotation” line will appear on the list below. Then click on the “Default” line in the lower list. The “Default” line disappears. It is important that before clicking in “ok”, the lists in the menu are the same as in figure 16. Finally click “apply”, and a DOS window appears. This can take several minutes. When the DOS windows disappears, the simulation is finished.



Figure 16: Subcase select menu for the analysis tab.

3.8.2 Batch run (several model run)

To be able to use the script from appendix A only one parameter needs to be changed. Setup the parameters as follows:

1. Action: Analyze
2. Object: Entire Model
3. Method: Method: Analysis Deck (this is the only parameter changed)

Do the same procedure with the “Subcase select” icon and click on apply. This time no DOS windows pops up. This will create a .bdf file in the Scratch folder with the “Job Name” as name. Run the Matlab script. A menu will pop up as in figure 17. Holding the “shift” key click on all the files you want to calculate and finally click on “open”. The computer will begin calculating all the simulations. This can take several hours.

The Matlab Command Window will indicate when it is finished with all the simulation files.

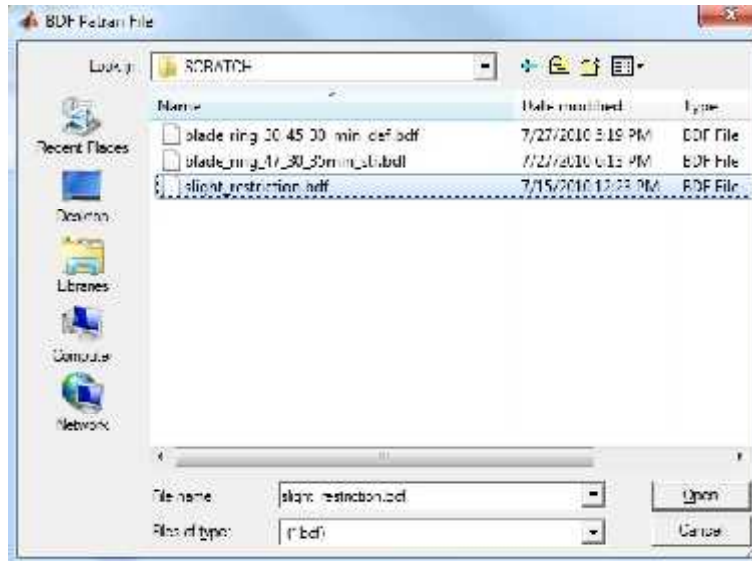


Figure 17: Matlab batch run script menu.

4 The Reference Model

The reference model is the model built from the technical sheets. The CAD model was built with the welding seams specified by the technical sheets, and every detail was modeled without any omission. Five different stress measuring positions were chosen given empirical data and the need to compare results with the different techniques developed later in the project (see figure 18).

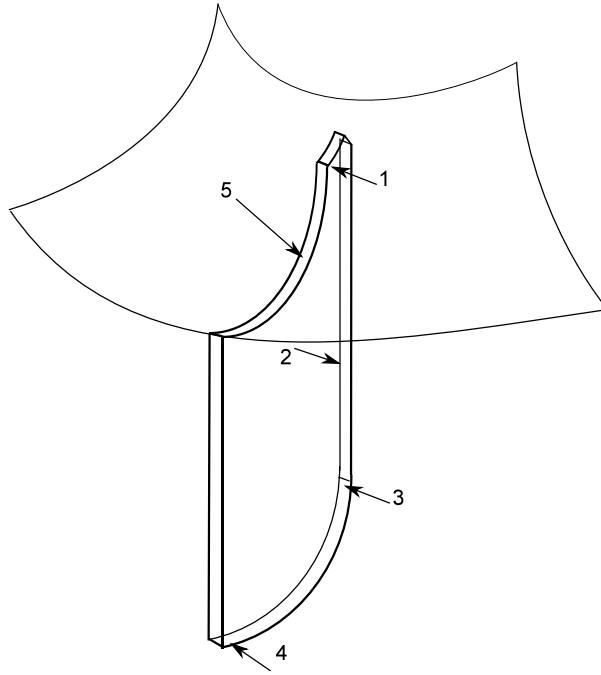


Figure 18: Stress measuring positions of the reference model.

On table 1 the stress results for the measuring points is given. The highest nodal displacement was given in position 2 and is 0.680 mm.

Blade Pos. 1	Blade Pos. 2	Blade Pos. 3	Blade Pos. 4	Top Ring Pos. 5
186	166	136	136	161

Table 1: Von Mises stress values of the reference model at given measuring points (MPa).

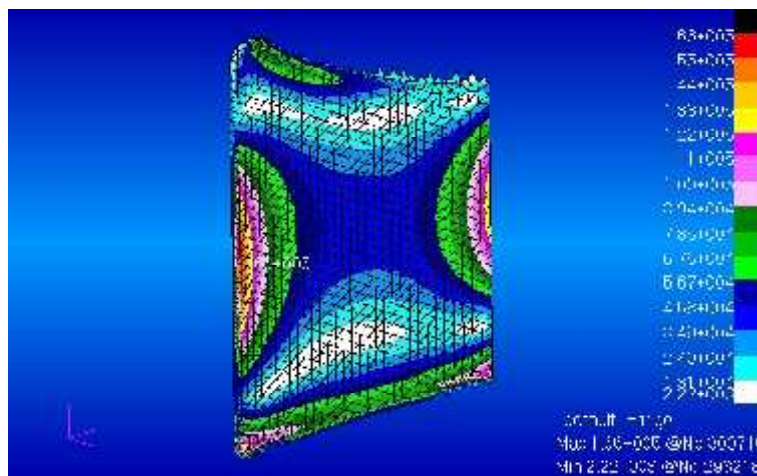


Figure 19: Von Mises stress distribution of the blade in the reference model.

5 Beads in the Top Ring

The top ring is the second component of the rotor that undergoes the highest stress values. Therefore adding beads to its geometry is of high interest.

5.1 Cross section and bead pattern

The bead pattern used in the top ring is a circular curve that runs along the top surface of the ring (see figure 21). An important reason to make this bead pattern is its ease to manufacture. The cross section of the bead is round-shaped. Figure 20 shows the parameters that describe such shape. They were calculated after Lange [19], being $R_{ST} = 7mm$, $h = 7mm$ and $R_z = 4.4mm$. The ring thickness t is equal to 3 mm from the technical sheets. These parameter values are considered conservative, since other authors give more extreme values.

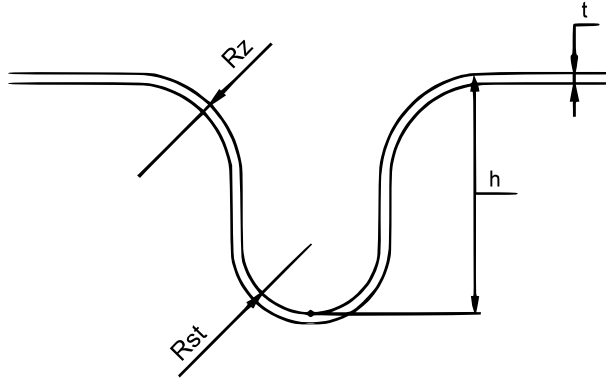


Figure 20: Cross section of round bead.



Figure 21: Bead pattern of top ring beads.

5.2 Variation of the bead pattern

Similar to the computer science algorithm “divide and conquer”, this method is used to vary the bead pattern. The goal of this variation is to minimize the Von Mises stress in the top ring,

or position 5 in figure 18.

5.2.1 Placing the first bead

The parameter varied from the bead pattern is the relative height of the circular curve to the bottom ring. This is better seen on figure 22.1. The first step of the algorithm is to do 3 simulations. On figure 22.2, these 3 simulations are the darkest 3 circles marked as 1,2 and 3. Between simulations 2 and 3, the Stress values are smaller as between 1 and 2. Therefore, a fourth simulation is done between 2 and 3. Between simulations 4 and 3 the stress values are smaller as between simulations 2 and 4. Finally, a fifth simulation is done between simulations 3 and 4. This is then the best place to construct the bead.

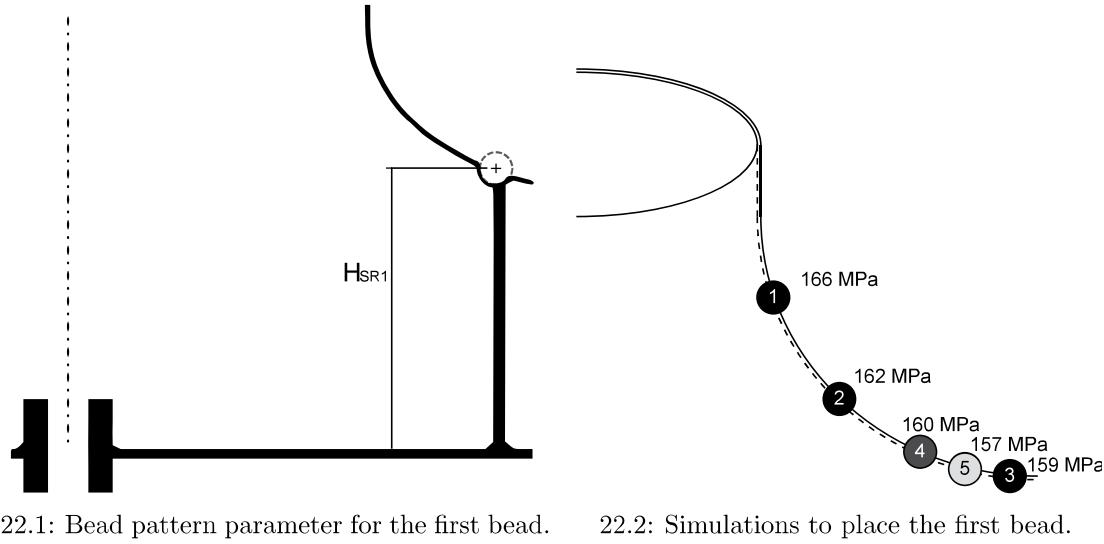


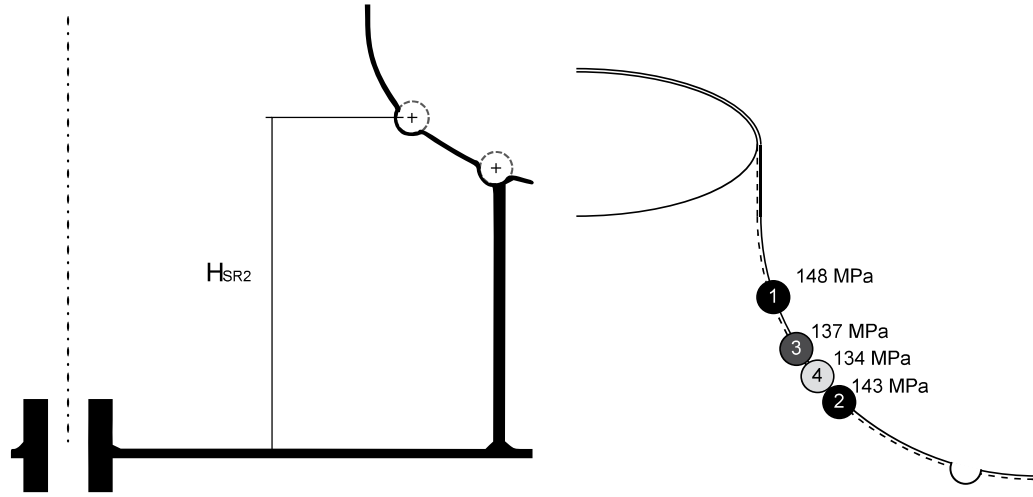
Figure 22: Placing of the first bead in the top ring.

5.2.2 Placing the second bead

Following the same algorithm as in section 5.2.1, the second bead is placed on the top ring. This is better explained by figure 7.6. It is important to highlight that all the simulations are done leaving the first bead in place.

5.3 Conclusions on placing beads on the top ring

After placing 2 beads on the top ring, a third bead had little or no effect in the stress values. The “divide and conquer” approach improved the stress values significantly. The overall Von Mises stress value improvement was of 17.2%. The top ring had an improvement of 21.1% and the blade 11.4%. The variables from figure 22.1 and 23.1 have a value of:



23.1: Bead pattern parameter for the second bead. 23.2: Simulations to place the second bead.

Figure 23: Placing the second bead in the top ring.

$$H_{SR1} = 200mm \quad H_{SR2} = 230mm$$

The rotor's global stress goes under in a smaller percentage as in the ring. This means that beading other places different from the top ring should improve local stress values as well as the global stress. Table 2 show the stress results with beads on the top blades on specific points of the rotors (see figure 18).

Blade Pos. 1	Blade Pos. 2	Blade Pos. 3	Blade Pos. 4	Top Ring Pos. 5
154	161	147	147	134

Table 2: Von Mises stress values after placing 2 beads on the top ring (MPa).



Figure 24: Von Mises stress distribution on the top ring after being beaded.

6 Beads in the Top Ring

After finding optimal Beads to manufacture in the top ring, beading the blade was also of interest. The method was carried on having the beads in place in the top ring from section 5.

6.1 Cross section and bead pattern

The cross section of the bead used is the same as in section 5.1. The bead pattern is calculated using spline curves on the surface of the bead surface. These splines have a predominant direction. Baumert et al. [20] found that beads that were oriented in the sense as the generatrix axis (vertical) had a positive effect on the stress values.

6.2 Placing of the first bead on the blade

The spline curve that lies on the bead has 3 knots (or spline points). Each node is restricted in 2 ways. The head of the spline is restricted a distance B_{r1} from the edge close to the generatrix. It is also a distance of 32 mm from the top ring (to avoid collisions with the beads on the top ring and to comply with specifications from Lange [19]).

The middle knot is a distance B_{r2} from the same edge as B_{r1} . In vertical direction, it is equally spaced from the head and the tail of the spline. Finally, the tail of the spline is a distance B_{r3} and is measured like B_{r1} . The tail is 32 mm apart from the bottom ring for the same reasons the head is from the top ring.

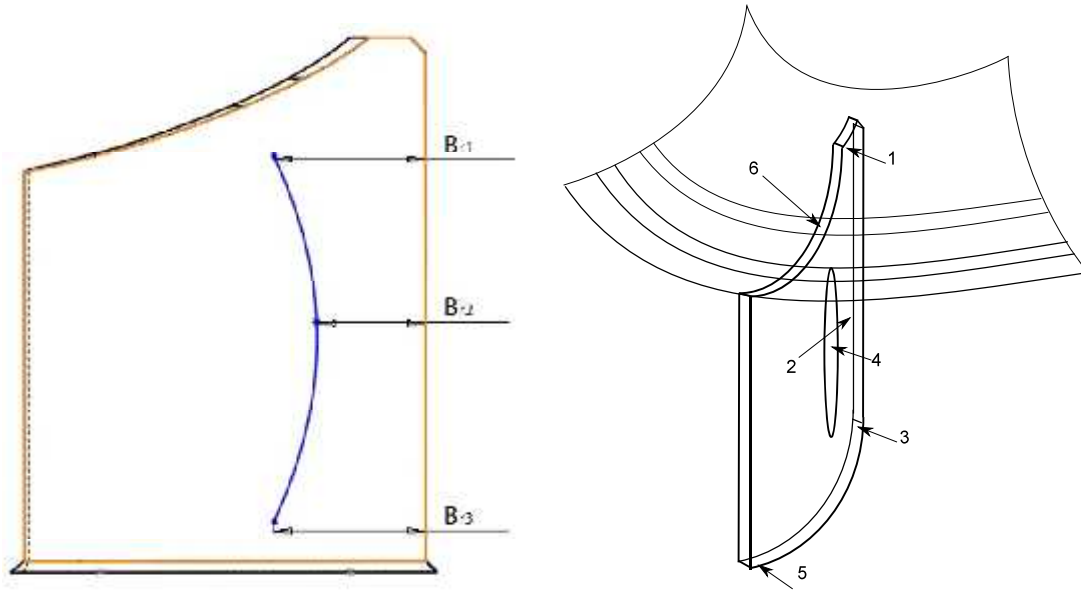
The distances B_{r1} , B_{r2} and B_{r3} vary 4 times. B_{r1} , B_{r2} , $B_{r3} = [30, 50, 70, 90]$. The possible combination of bead patterns is 4^3 , or 64. This variation of the spline's knot positions will be called from now on as "the snake algorithm". This name is used since the movement of the spline in the surface resembles the movement of a snake on a surface.

6.3 Results after placing the first bead on the blade

After simulating the 64 models with the different bead patterns, the best shape found was when:

$$B_{r1} = 30mm \ B_{r2} = 30mm \ B_{r3} = 30mm$$

From figure 26 it can be inferred that the stress distribution is more uniform in the blade's surface. Comparing the stress distribution from the unbeaded model (Figure 19) and the beaded model (figure 26), it is clear that the stress in the edges of the blades diminishes as



25.1: Parameters of the first bead pattern on the blade. 25.2: Measuring positions of the first bead on the blade model.

Figure 25: Parameters and measuring positions for placing the first bead on the blade.

beads are added. This gives a hint on how the beadings work on the blade. The offset geometry of the bead adds more Inertia to the blade, but this point also suffers a higher stress value, since it is further away from the neutral fibers of the blade. It also indicates that the rotor is closer to achieving a full-stressed design.

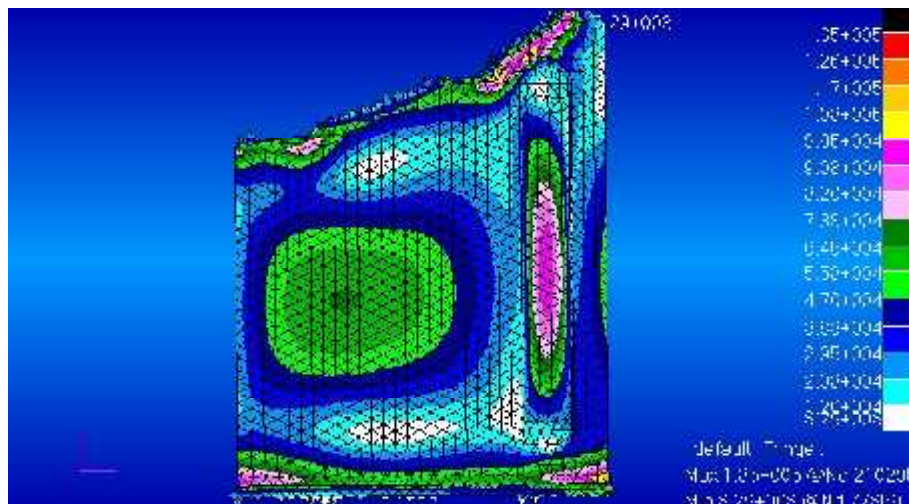


Figure 26: Von Mises stress distribution in the blade after adding one Bead.

The Von Mises stress values from the points in figure 25.2 can be seen in table 3. The highest Von Mises stress value is 137 MPa in position 5.

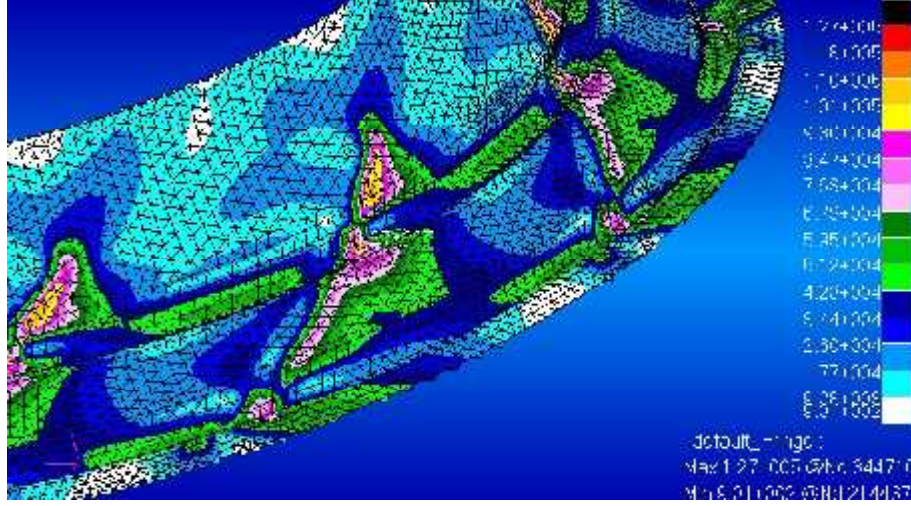


Figure 27: Von Mises stress distribution in the top ring after adding one bead.

Blade Pos. 1	Blade Pos. 2	Blade Pos. 3	Blade Pos. 4	Blade Pos. 5	Top Ring Pos. 6
130	117	119	98	137	127

Table 3: Von Mises stress values after placing 1 bead on the blade.

6.4 Placing of the second bead on the blade

Using the same methodology for placing the first bead (section 6.2), a second bead was placed on the blade. The variable names were changed to B_{l1} , B_{l2} , B_{l3} . The edge from where the variables are measured to the spline's knots are changed as well. This time the reference edge is the outermost edge of the blade when compared to the generatrix. This is better explained by figure 28.1.

The bead pattern found previously is left in its place. A new set of 64 simulations is done with the same variable values (30, 50, 70 and 90).

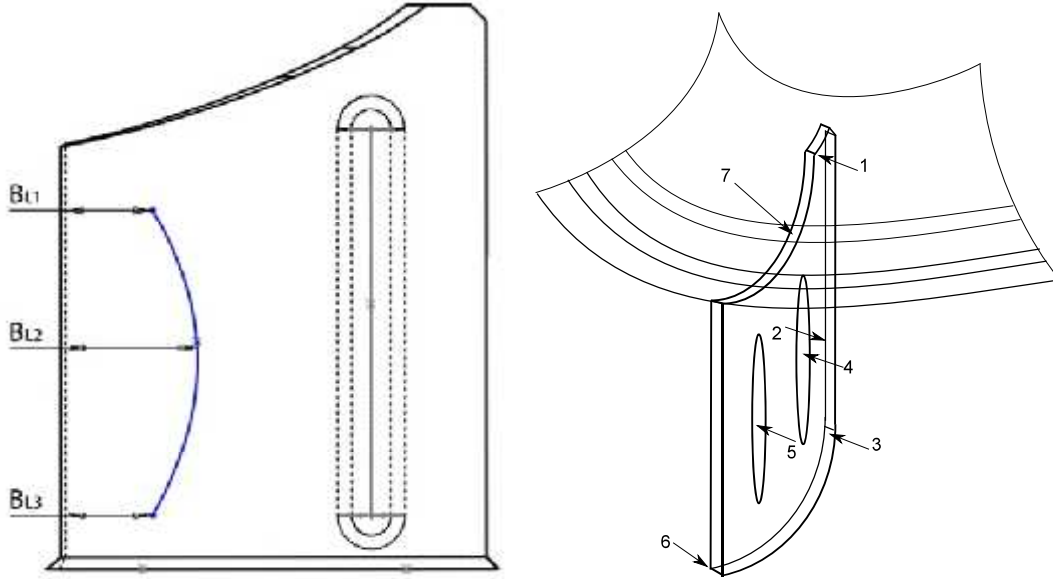
6.5 Results after placing the second bead on the blade

The best bead pattern found for the second bead was:

$$B_{l1} = 30mm \ B_{l2} = 50mm \ B_{l3} = 30mm$$

The highest Von Mises stress value is 125 MPa. Different from the 1 bead model, the highest stress place was position 1.

From figure 29 it can be seen that the top of the beads are the places with highest stress values in the blade. This is a characteristic found from all the simulations that lowered the Von Mises



28.1: Parameters of the second bead pattern on the blade
 28.2: Measuring positions of the second bead on the blade model.

Figure 28: Parameters and measuring positions for placing the second bead on the blade.

Blade P. 1	Blade P. 2	Blade P. 3	Blade P. 4	Blade P. 5	Blade P. 6	Top Ring P. 7
125	111	125	102	101	90	125

Table 4: Von Mises stress values after placing 2 beads on the blade.

stress. Another characteristic is that these stress values would have similar values in both bead's top.

6.6 Conclusion for the beads on the blades

When the first bead is placed, the stress values go under considerably. When the second one is placed, the stress values aren't greatly affected. This can be better seen comparing the spheres diagrams of both beads.

A sphere diagram is a way to represent 4 dimensional information. In figure 31 there is 64 spheres. Each sphere represents a simulation from section 6.2, where the first bead pattern was found. The color of the sphere represents the maximum stress value of the rotor. Figure 32 shows the maximum stress values for the placing of the second bead. It can be seen that after placing the second bead many simulations have similar results as the best from the first bead.

The use of a second bead could be unnecessary when the design goal is to lower the maximum stress values. The analysis of the bead pattern with other goals such as deformation minimization or modal analysis could find useful the use of a second bead.

Using the "snake algorithm" proved to be a good way to calculate the bead pattern to be

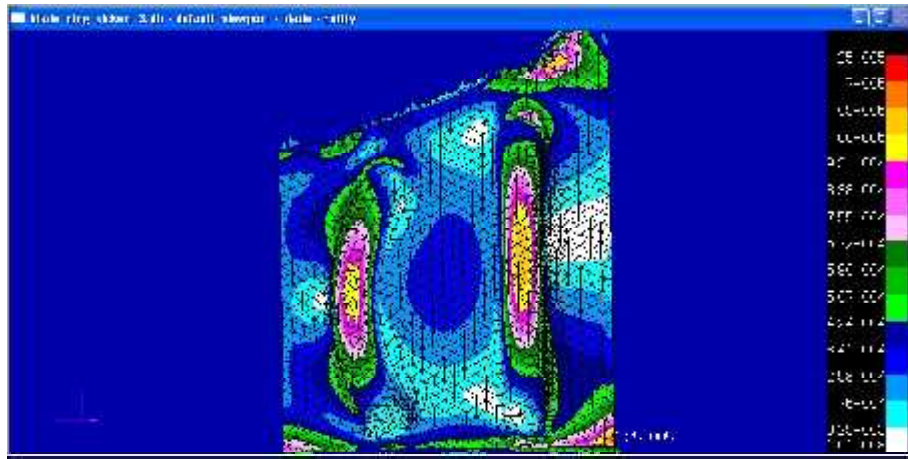


Figure 29: Von Mises stress distribution in the blade after adding two beads.

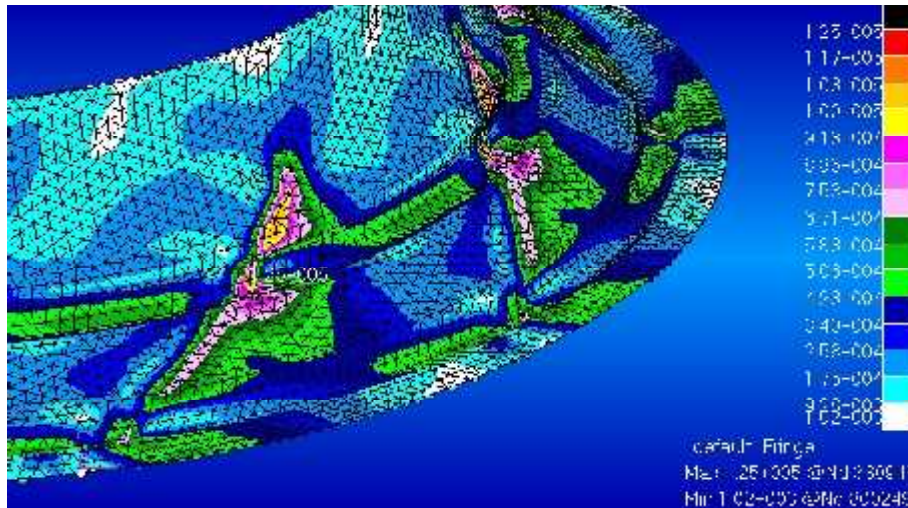


Figure 30: Von Mises stress distribution in the top ring after adding two beads.

used on a metallic sheet. One of the biggest advantages of using this methodology is that it relies mostly on the abilities of the user to create CAD software. Other methodologies rely on the user's computer programming capabilities and the difficult interaction between programs different from the CAD and CAE software.

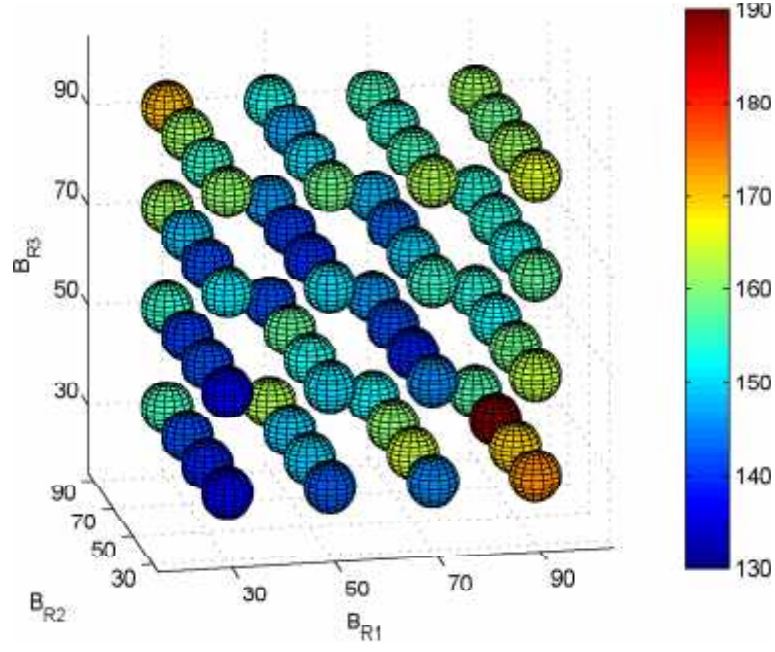


Figure 31: Sphere diagram of 64 simulations to find the best bead pattern for the one-beaded model.

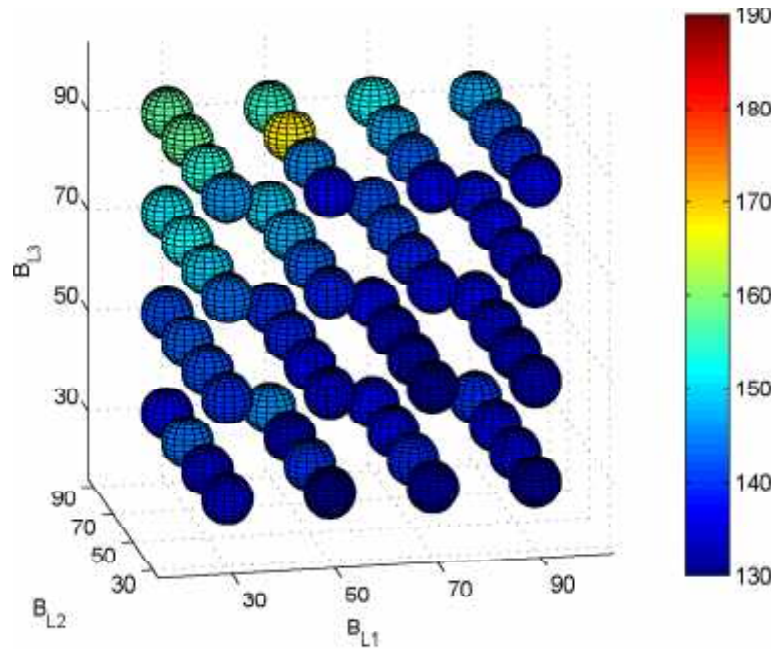


Figure 32: Sphere diagram of 64 simulations to find the best bead pattern for the two-beaded model.

7 Optimization of Bead Patterns Using Design of Experiments

On section 6, a trial and error approach was used. This type of approach is very time and resource consuming. For that reason the implementation of a true optimization method was interesting to do.

The optimization problem can be defined in 3 different ways. The first one finds the bead shapes that minimizes the maximal Von Mises Stress in the entire model (equation 7 and 9). The second one finds the bead shapes that minimizes the maximal nodal displacement in the entire model (equation 8). The last one finds the stress in specific points (as in figure 25.2)

$$\min (\sigma_r (x)) \quad (7)$$

$$\min (d_r (x)) \quad (8)$$

$$\max (\min (\sigma_1 (x)), \min (\sigma_2 (x)), \dots, \min (\sigma_i (x)), \dots, \min (\sigma_p (x))) \quad (9)$$

The function $\sigma_r : R^3 \rightarrow R$ is the maximum Von Mises Stress value of the entire rotor geometry according to Patran's GUI (the location of this point can change in the geometry). The function $d_r : R^3 \rightarrow R$ is the maximum displacement function of the entire model according to Patran's GUI (this point is always in the middle of the blade). The function $\sigma_i : R^3 \rightarrow R$, for $i = 1, 2, \dots, p$. This function is the Von Mises Stress value in specific points p on the rotor according to figure 25.2. The functions σ_r , d_r and σ_i are also known as the observed phenomena (experimental values). The vector $x = [B_{r1}, B_{r2}, B_{r2}]$ in the case of the placement of the first bead.

7.1 4 level 3 factors experiment design

This type of design was chosen for 3 reasons:

- i The function that describes the bead patterns in the blades is unknown. 4 levels would approximate accurately a cubic function and won't affect smaller order polynomials.
- ii The 3 factors would be the spline's control points.
- iii There is a very good statistical data from the previous sections.

Similar to equation 4, equations 10, 11 and 12 show the lineal, quadratic and cubic polynomials for 3 variables. As explained in section 1.5, the challenge is to find the independent terms a_i .

$$S_a^1(x) = a_1 + a_2x_1 + a_3x_2 + a_4x_3 + e \quad (10)$$

$$S_a^2(x) = S_a^1 + a_5x_1x_2 + a_6x_1x_3 + a_7x_2x_3 + a_8x_1^2 + a_9x_2^2 + a_{10}x_3^2 \quad (11)$$

$$S_a^3(x) = S_a^2 + a_{11}x_1x_2x_3 + a_{12}x_1^2x_2 + a_{13}x_1^2x_3 + a_{14}x_1x_2^2 + a_{15}x_2^2x_3 + a_{16}x_1x_3^2 + a_{17}x_2x_3^2 + a_{18}x_1^3 + a_{19}x_2^3 + a_{20}x_3^3 \quad (12)$$

7.1.1 Choosing which tests to run

The Box-Wilson Central Composite Design and the Box-Behnken Design are not good describing the 4 levels experiments. The approach by Koukouvinos et al. was used [21], where optimal non-orthogonal designs were created using neural algorithms. Figure 33.1 shows for example a 20 run (simulations), 4 level, 3 factors design. A full factorial design would have all the dots in the matrix black. Full factorial designs are further explained by Woll et. al. [22].

When the experiments are carried out, the lineal equation systems are built like in equations 10,11, 12 and the polynomials coefficients of the response surface are found as in equation 5.

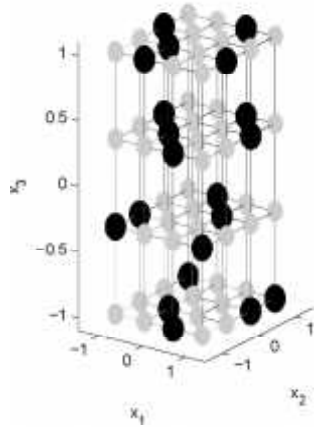
7.1.2 Measuring the goodness of fit from the polynomials

One parameter that has been widely used to measure the quality of the polynomial fit is called R squared (coefficient of determination or R^2) [23]. Equation 13 shows the calculation of such parameter for the Maximum Von Mises stress, when the hyper-surface S_a^n is approximated. The parameter i is the number of runs used and depends on the experimental design used.

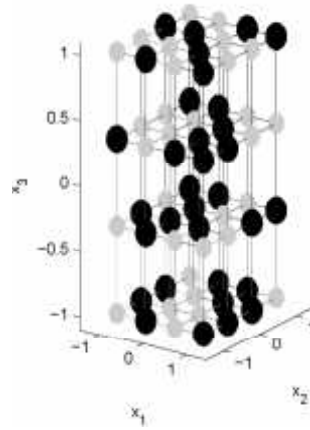
$$R^2 = 1 - \frac{\sum_i (\sigma_r(x_i) - S_a^n(x_i))^2}{\sum_i (\sigma_r(x_i) - \overline{\sigma_r(x)})^2} \quad (13)$$

R^2 is an adimensional number, that should have values between 0 and 1. When the value is closest to 1, the approximation of the response surface is better. There is not a minimum value that is good to ensure the correctness of the response surface, but values of 0.6 in this project have given satisfying results.

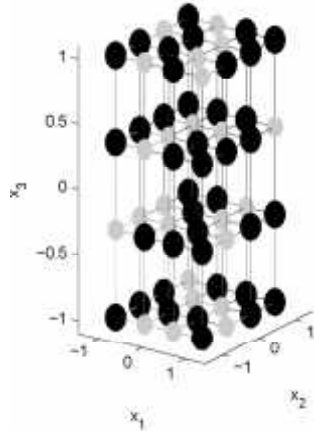
The displacement function (d_r) approximations had the highest coefficient of determination (see figure 34.2). The smallest values were found when approximating the σ_r function. The σ_i approximations had good R^2 values (see figures 34.1 and 34.4). There were no major differences in the R^2 values between the second and third degree polynomials in all the approximations as the number of runs increases (converged to equal values). The third degree polynomials had



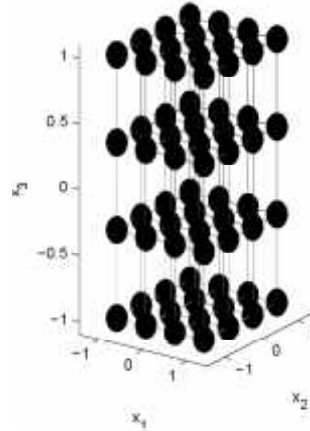
33.1: 20 runs design of experiments.



33.2: 36 runs design of experiments.



33.3: 48 runs design of experiments.



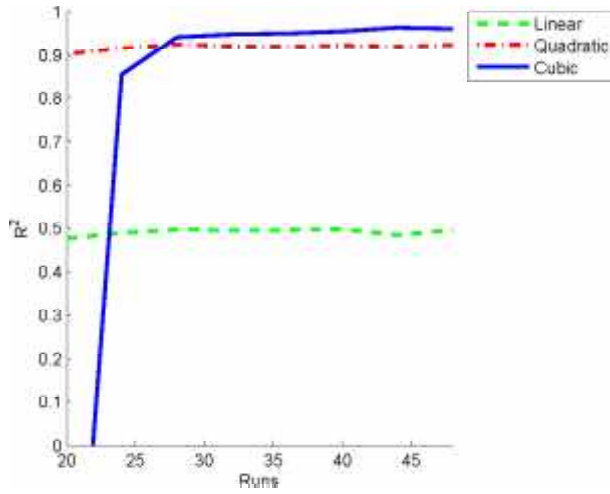
33.4: 64 runs (Full Factorial design of experiments).

Figure 33: Different design of experiments in a 4^3 space according to Koukouvinos

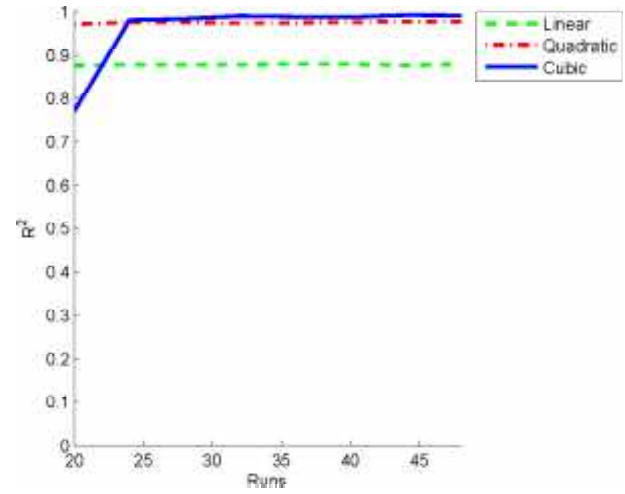
low or negative R^2 values with low runs number, but at high run numbers they would have the highest.

7.2 Results using 20 runs design

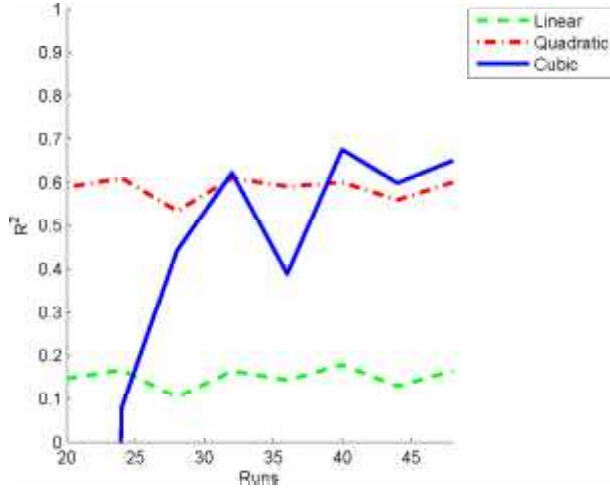
It is only interesting to show the approximations using the 20 runs experiment design, since the goal of this chapter is to diminish the amount of simulations needed to determine the optimum bead pattern in the blade. Figure 35 through figure 38 show the variations of vector $x = [B_{r1}, B_{r2}, B_{r1}]$ in the domain used on section 6. The colormap represent the value of the hyper-surface S_a^n at used to approach the different Stress and Deformation functions at a point x .



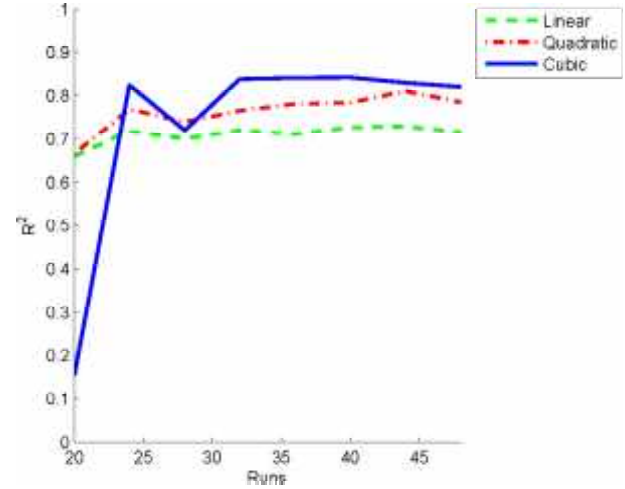
34.1: R^2 values of the polynomials that fit the Stress values in the middle of the blade.



34.2: R^2 values of the polynomials that fit the nodal displacement data.



34.3: R^2 values of the polynomials that fit the maximum stress values.



34.4: R^2 values of the polynomials that fit the Stress values in the top of the bead.

Figure 34: Measuring the goodness of fit for different polynomials from measurement data in the fan's rotor.

7.2.1 Polynomials describing Maximum Stress Values in the Rotor

After finding the response surface approximations, the minimal values for each polynomial in the domain of x were found. Table 5 shows the predicted optimum values and the value of the components of x .

The Quadratic polynomial prediction was tested, and the Von Mises stress value is 137 MPa. This means that the prediction was accurate, and matches the best result found in section 6. This is the solution for equation 7. The best approximation is given by the cubic approach with 64 runs with a R^2 value of 0.83 (see figure 35.4). There are weak similarities between the approximations with 20 runs and the best approach.

Polynomial Used	Predicted B_{r1} (mm)	Predicted B_{r2} (mm)	Predicted B_{r3} (mm)	Predicted Max. Stress(MPa)
Linear	30	30	30	143
Quadratic	47	30	35	135
Cubic	30	90	58	105

Table 5: Predicted minimum values for the σ_r function and the bead pattern parameters.

7.3 Polynomials describing Stress Values in positions 2 and 4

This approach is an example of solving the optimization problem in equation 9. In figure 25.2, the positions 2 and 4 are shown. These are called “the middle of the blade” and “top of the bead”. It is known by empirical data that the failing zone of the rotor is the middle of the blade. Both points 2 and 4 go through the empirical failing area, and were chosen for this reason.

Polynomial Used	Predicted B_{r1} (mm)	Predicted B_{r2} (mm)	Predicted B_{r3} (mm)	Predicted Max. Stress(MPa)
Linear	30	90	30	89
Quadratic	30	63	41	84
Cubic	88	39	30	62

Table 6: Predicted minimum values for the σ_2 function and the bead pattern parameters.

Polynomial Used	Predicted B_{r1} (mm)	Predicted B_{r2} (mm)	Predicted B_{r3} (mm)	Predicted Max. Stress(MPa)
Linear	30	30	30	109
Quadratic	30	30	30	108
Cubic	30	30	30	83

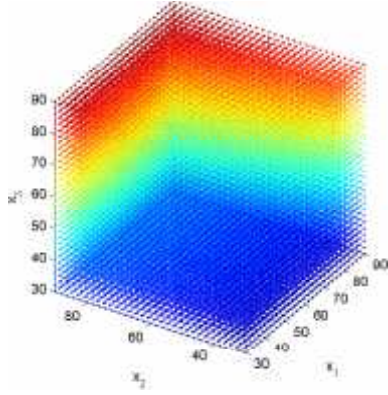
Table 7: Predicted minimum values for the σ_4 function and the bead pattern parameters.

When comparing the results of the Quadratic approximation in tables 6 and 7, the maximum Von Mises stress values is 108 in the σ_4 function. The bead pattern is the same as in section 6.3. This is the bead pattern that solves the optimization problem stated in equation 9.

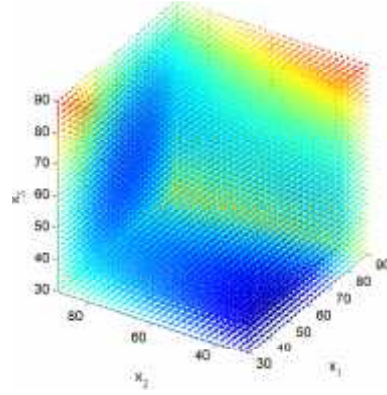
The best possible approaches were using cubic polynomials with 64 runs (figure 36.4 and 37.4). The R^2 values was 0.99. When there is a comparison between the cubic approaches and the quadratic approaches with only 20 runs, the similarity is evident. This makes the quadratic approach reliable.

7.3.1 Polynomials describing Maximum Deformation Values

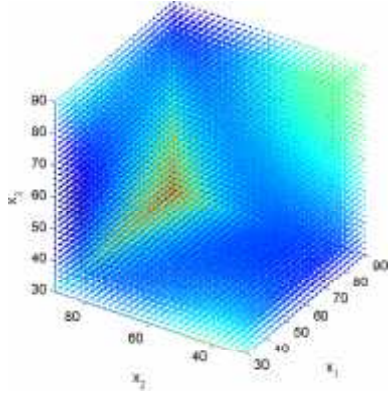
The polynomials that approach the deformation are the best behaving ones. This can be seen by the likeness of figure 38.1 through figure 38.4. The predictions using the quadratic polynomial



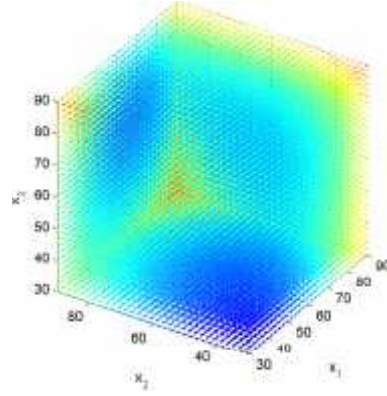
35.1: Linear polynomial approximation of σ_r with 20 runs.



35.2: Quadratic polynomial approximation of σ_r with 20 runs.



35.3: Cubic polynomial approximation of σ_r with 20 runs.



35.4: Cubic polynomial approximation of σ_r using 64 runs (full factorial design).

Figure 35: Linear, Quadratic and Cubic approximations of the σ_r function.

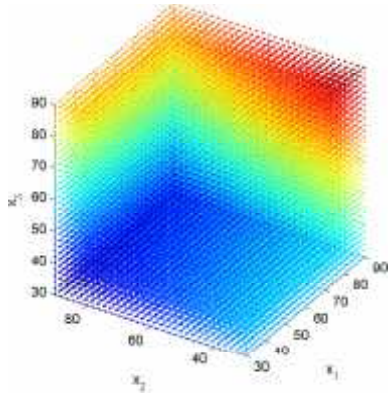
with 20 runs was 100% accurate when the verification was made.

Polynomial Used	Predicted B_{r1} (mm)	Predicted B_{r2} (mm)	Predicted B_{r3} (mm)	Predicted Max. Disp (mm)
Linear	30	30	30	0.352
Quadratic	30	45	30	0.348
Cubic	30	63	34	0.340

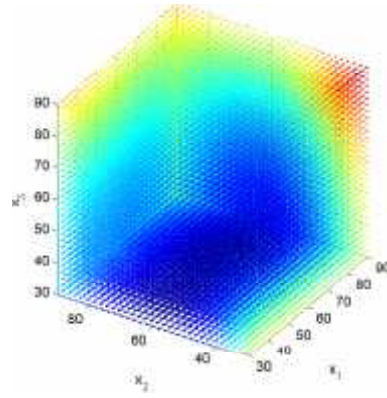
Table 8: Predicted minimum values for the d_r function and the bead pattern parameters.

7.4 Conclusion of Creating Bead Patterns Using Design of Experiments

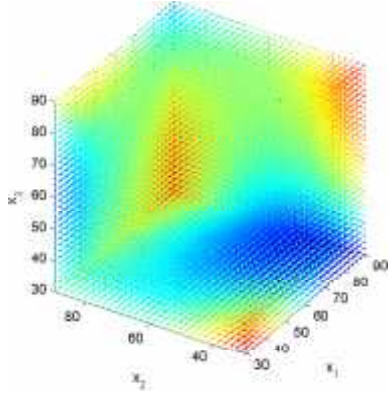
The use of design of experiments to find bead patterns is a powerful tool that proved to be accurate and time saving. The snake algorithm was improved using less than one third of the



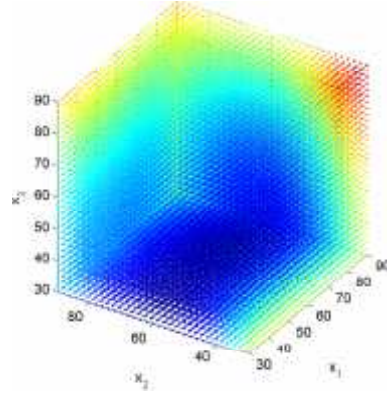
36.1: Linear polynomial approximation of σ_2 with 20 runs.



36.2: Quadratic polynomial approximation of σ_2 with 20 runs.



36.3: Cubic polynomial approximation of σ_2 with 20 runs.



36.4: Cubic polynomial approximation of σ_2 using 64 runs (full factorial design).

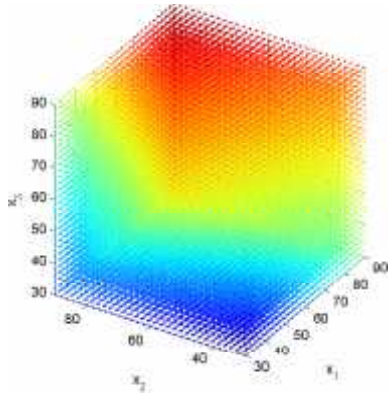
Figure 36: Linear, Quadratic and Cubic approximations of the σ_2 function.

time and resources. In the case of forecasting nodal displacement, the results are better than using the actual snake algorithm.

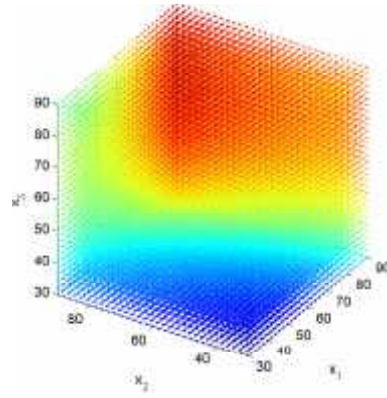
Using response surfaces in a closed domain brings the possibility of finding several minimal values. Therefore using design of experiments could be useful to find not only one bead pattern that minimizes the stress values, but several. Then the user must choose which pattern is easier to manufacture or if there are additional functionalities that give advantages of some patterns over others (in the fan, some patterns might produce less turbulence as others).

From the color distribution in figure 39 and 40, it can be concluded that the full-stressed design can be extended to nodal displacement as well. The concentration seen in the unbeaded model can now be seen in two different places in the beaded model. It can be seen as well that the highest displacement values in the beaded model tends to become equal in the horizontal direction. The nodal displacement was lowered by 51%.

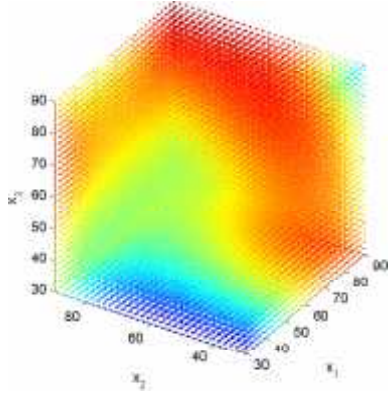
Comparing the distribution of the Von Mises stress on the beaded and unbeaded blade (figure



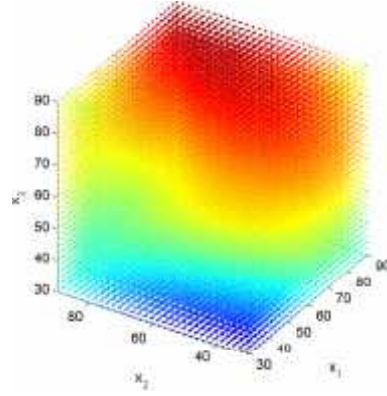
37.1: Linear polynomial approximation of σ_4 with 20 runs.



37.2: Quadratic polynomial approximation of σ_4 with 20 runs.



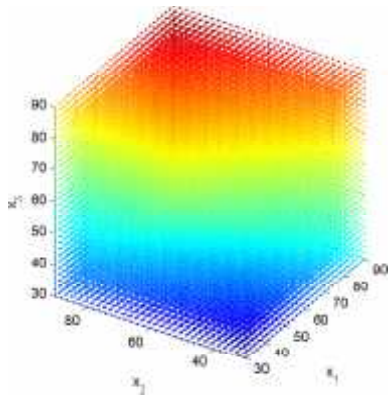
37.3: Cubic polynomial approximation of σ_4 with 20 runs.



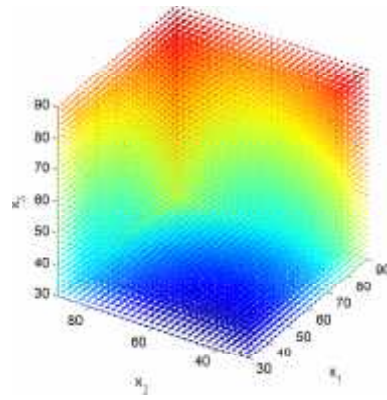
37.4: Cubic polynomial approximation of σ_4 using 64 runs (full factorial design).

Figure 37: Linear, Quadratic and Cubic approximations of the σ_4 function.

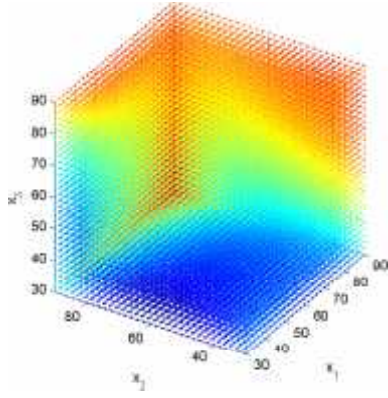
41 and 42) there is no immediate difference. Looking closer, in the beaded blade both extreme edges in the middle of the blade have the similar stress values, while the unbeaded blade has a clear concentration on the inner edge. The highest stress value changed from the middle of the blade to the lowest outer weld.



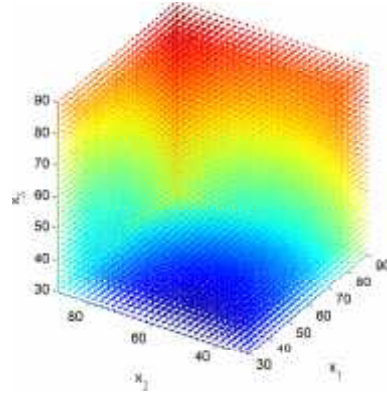
38.1: Linear polynomial approximation of d_r with 20 runs.



38.2: Quadratic polynomial approximation of d_r with 20 runs.



38.3: Cubic polynomial approximation of d_r with 20 runs.



38.4: Cubic polynomial approximation of d_r using 64 runs (full factorial design).

Figure 38: Linear, Quadratic and Cubic approximations of the d_r function.

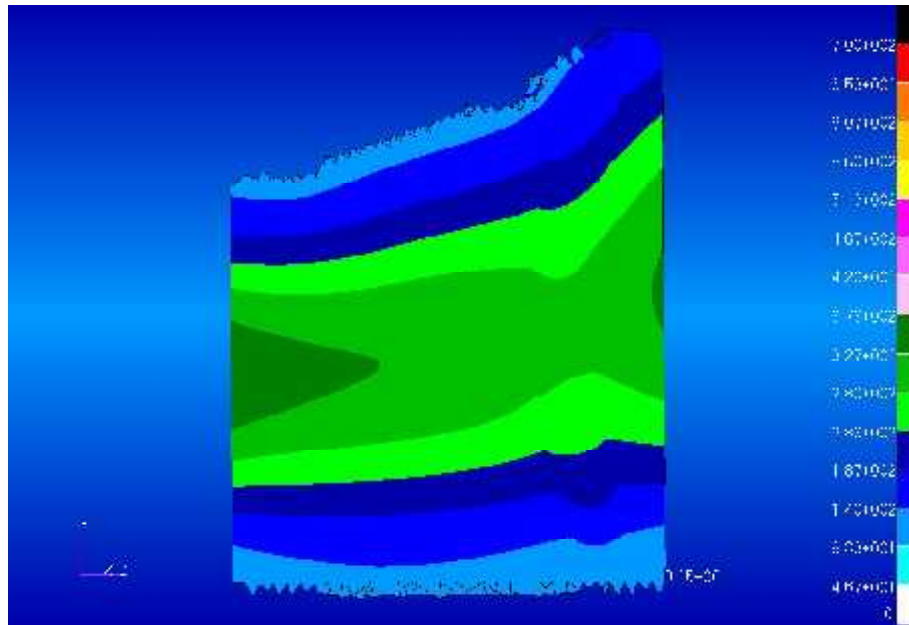


Figure 39: Optimized bead beaded blade with nodal displacement colormap.

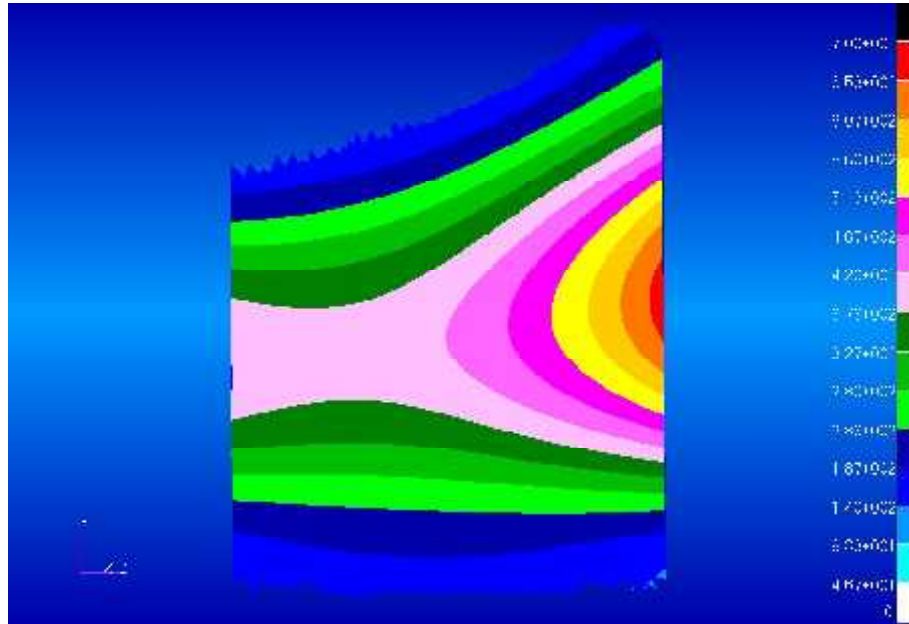


Figure 40: Unbead blade with nodal displacement colormap.

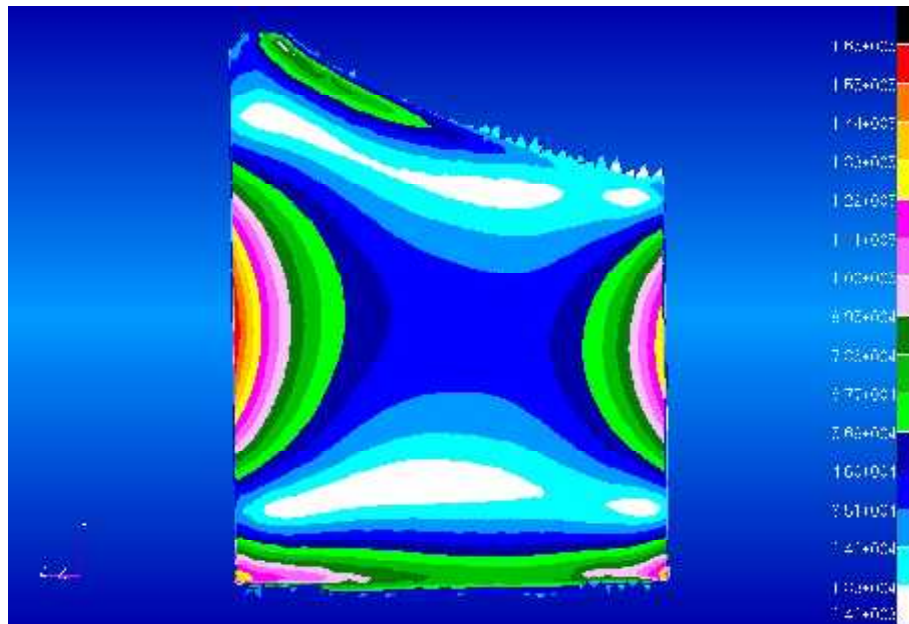


Figure 41: Back view of the unbeaded blade with Von Mises colormap.

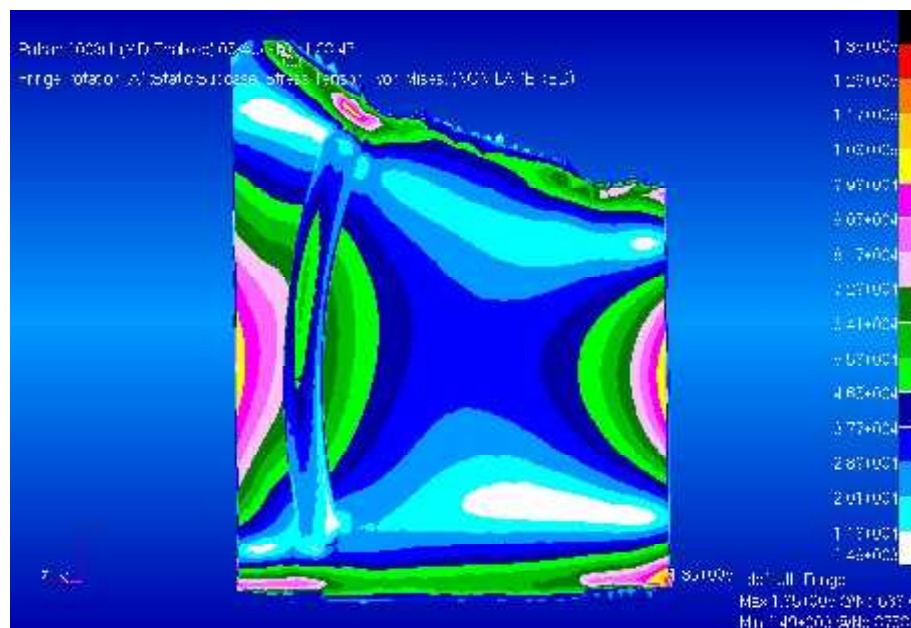


Figure 42: Back view of the optimized bead beaded blade with Von Mises colormap.

8 Optimizing the Bead's Cross Section

In the previous sections, the best bead contour was found. The parameters for the bead pattern are taken from section 6. It is believed that the bead pattern is predominant from the bead cross section. For this reason, the cross section optimization is done after finding an appropriate bead pattern.

The cross section of the bead has different parameters. Any type of bead (rectangular, triangular, circular, trapezoidal) can be described using the same parameters. They are:

1. w : Width of the bead
2. h : Depth of the bead
3. Rad : Forming Radius of the bead.
4. β : Forming angle of the bead.
5. t : Thickness of the metal sheet.

On figure 43 the parameters are shown. These parameters were varied with common values found in literature [7], [24], [19]. These values are:

$$w = [16, 18, 20, 22]\text{mm}; h = [7, 9, 11]\text{mm}; Rad = [3, 5]\text{mm}; \beta = [45, 60, 75, 90];$$

The parameter t is given previously by the technical sheets from the rotor.

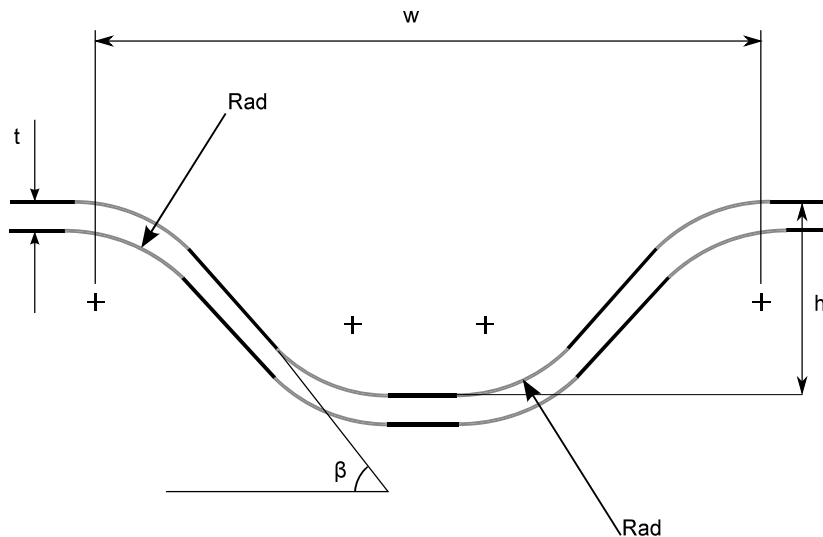


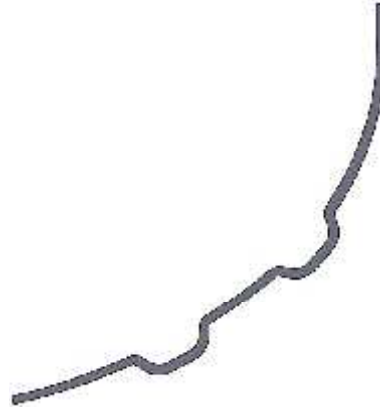
Figure 43: Global parameters of a bead's cross section.

The use of different types of Beads is shown by [25]. He concludes that the box-shaped beads ($\beta = 90$ degrees) have the highest stiffening effect; although [26] briefly discusses the problems inherent to metal sheet forming in right angles. Due to geometrical restrictions, some parameter combinations are not possible to build.

Special attention was paid to the β angles of 60 and 90 degrees beads, because just like round-shaped beads, these are the most common ones. Figure 44.1 through 44.4 show a cross section of the top ring with the geometry of the bead. The only parameter changed between the models was the β angle. The change is easy to see comparing the initial and the last figure, but the transition in between is difficult to appreciate.



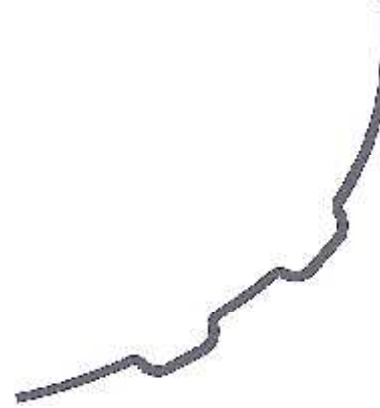
44.1: Generatrix of $\beta = 45$ model.



44.2: Generatrix of $\beta = 60$ model.



44.3: Generatrix of $\beta = 75$ model.



44.4: Generatrix of $\beta = 90$ model.

Figure 44: Top ring generatrix with varying β angle.

8.1 Stress concentration due to small Rad parameter values

Figure 45 and 46 share the same parameter values except the forming radius (Rad). It can be clearly seen that even though Kugler [26] states that the Rad parameter can have a values of 3 mm in the case of the fan's rotor high stress concentrations are found. It is therefore

recommendable to avoid small values in this instance. The 5 mm value was found to be a good value. Larger values are difficult to build since it restricts the amount other parameters can change.

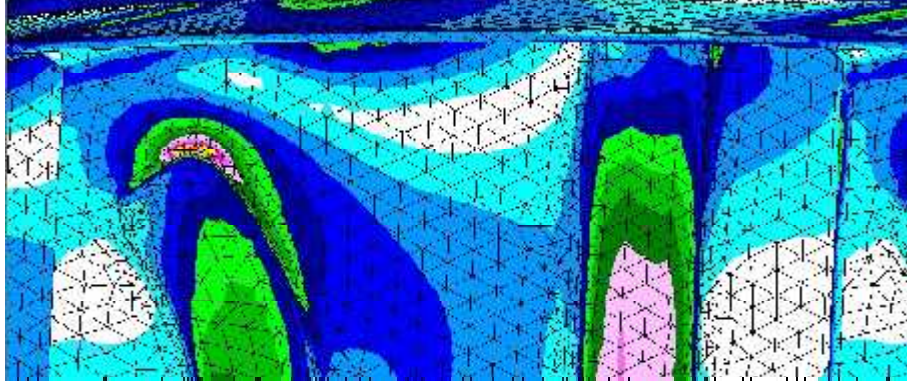


Figure 45: Model with parameter $Rad = 3$ mm

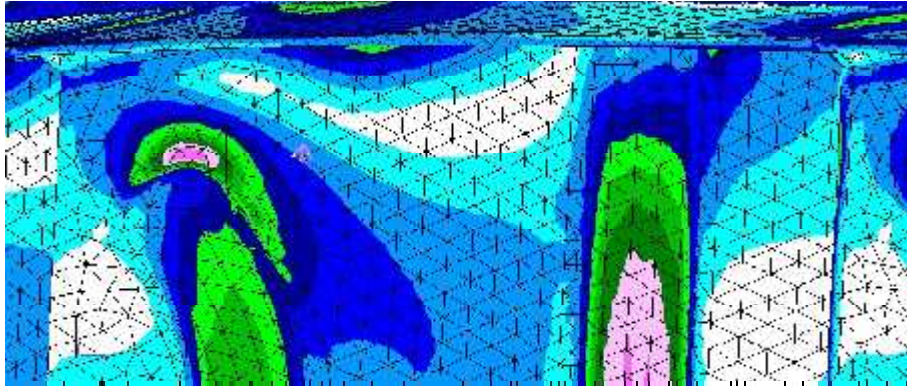
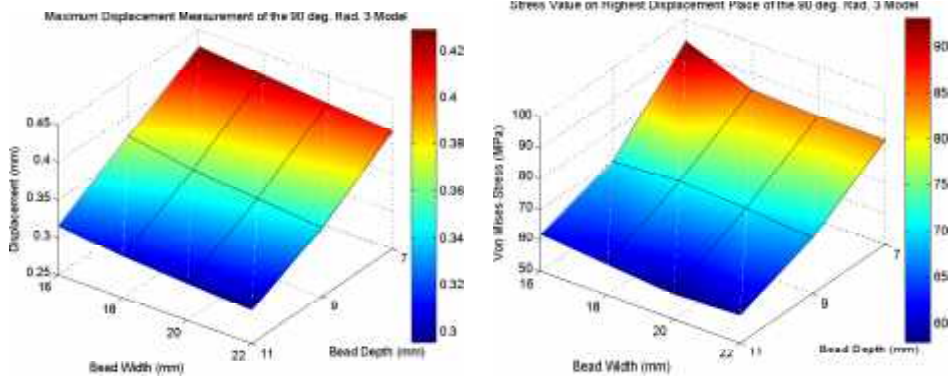


Figure 46: Model with parameter $Rad = 5$ mm

8.2 Constant $\beta = 90$ degree and $Rad = 3$ varying h and w

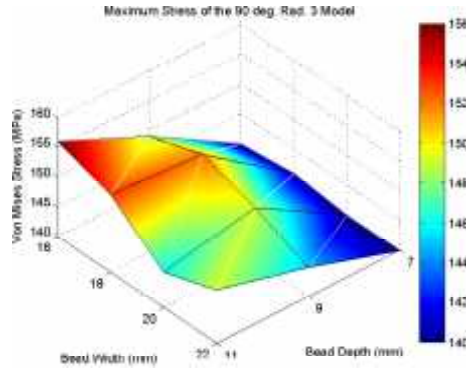
From the maximum stress values surface (figure 47.3) there are results that go against the theory. The stress values are supposed to reduce as the bead is deeper. This behavior was found to occur when the Rad parameter is too small. There are stress concentrations with this value. The use of shallower beads are better. The use of 3 mm in this parameter proved to be too small, and therefore it wasn't further explored.

The values of deformation did behave accordingly to the theory (figure 47.1) and the stress value in the middle of the blade too (47.2).



47.1: Maximum nodal displacement of the 90 degree, $Rad = 3$ models.

47.2: Stress values at highest displacement point of the 90 degree, $Rad = 3$ models.



47.3: Maximum Stress of the 90 degree, $Rad = 3$ models.

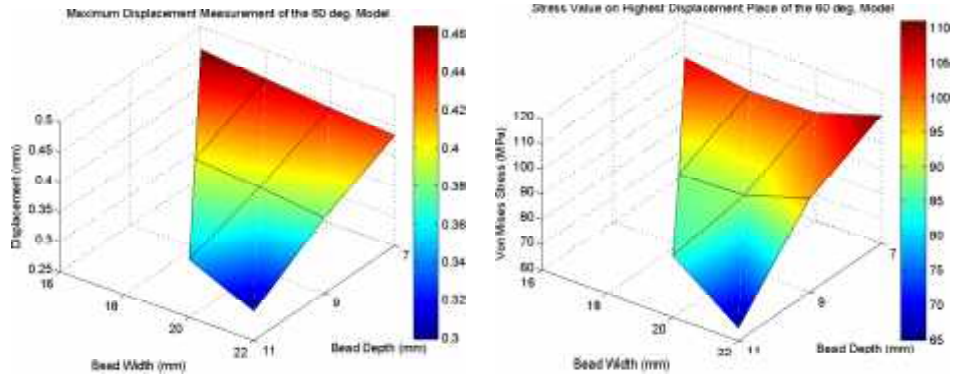
Figure 47: Surfaces describing the Stress and Nodal Displacement behavior of $\beta = 90$ degree and $Rad = 3$ models.

8.3 Constant $\beta = 60$ degree and $Rad = 5$ varying h and w

There are no stress or displacement values in some width and depth values (i.e. $h = 11$, $w = 16$) in the graphic because they are not geometrically possible to construct. The surfaces are not completely lineal. The height is the dominant parameter, but it's difficult to establish whether the width plays a major role because the surfaces don't have enough test points.

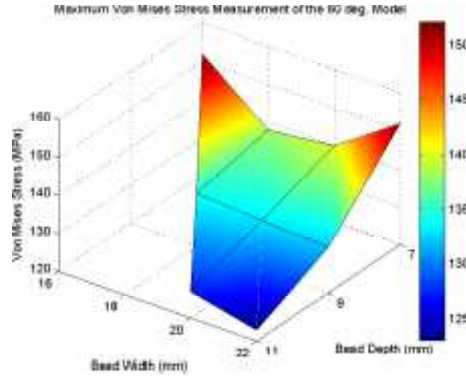
8.4 Constant $\beta = 90$ degree and $Rad = 5$ varying h and w

On these models, the Rad and β parameters are constant and the width and depth vary. The results have a linear behavior and there are no local minima. The bead depth is the dominant parameter. These models had the most consistent behavior.



48.1: Maximum nodal displacement of the 60 degree, $Rad = 5$ models.

48.2: Stress values at highest displacement point of the 60 degree, $Rad = 5$ models.



48.3: Maximum Stress of the 60 degree, $Rad = 5$ models.

Figure 48: Surfaces describing the Stress and Nodal Displacement behavior of $\beta = 60$ degree and $Rad = 5$ models.

8.5 Influence of the β angle

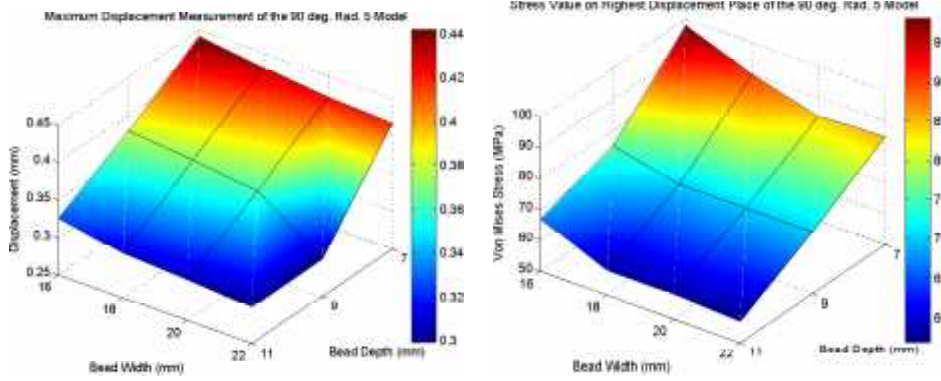
On figure 50.1 it can be seen that the maximum displacement of the rotor gets lower as the β angle grows. Different from the displacement, the Stress values are not continuously falling (see figure 50.2). There is a local minimum when β is equal to 60 degrees. This is the main reason why there was more attention paid to the 60 and 90 degrees β angles.

The nodal displacement between the 60 and 90 degrees models are slightly different, being always lower the 90 degree model (see figure 51).

8.6 Conclusion for Bead Cross Section Optimization

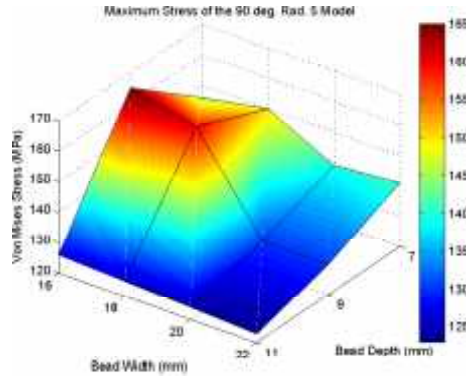
The Best model found was the squared-shaped bead with the following parameters:

$$w = 22 \text{ mm}; h = 11\text{mm}; Rad = 5\text{mm}; \beta = 90 \text{ deg.}$$



49.1: Maximum nodal displacement of the 90 degree, $Rad = 5$ models.

49.2: Stress values at highest displacement point of the 90 degree, $Rad = 5$ models.



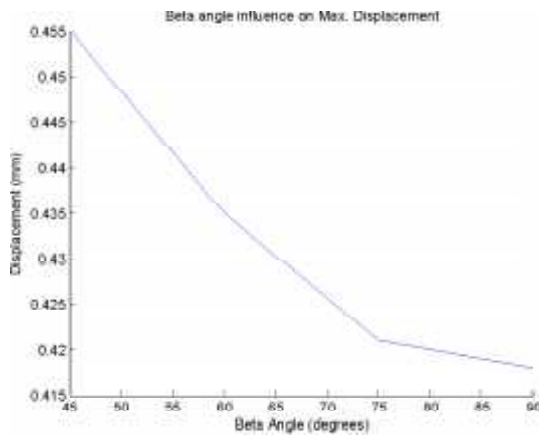
49.3: Maximum Stress of the 90 degree, $Rad = 5$ models.

Figure 49: Surfaces describing the Stress and Nodal Displacement behavior of $\beta = 90$ degree and $Rad = 5$ models.

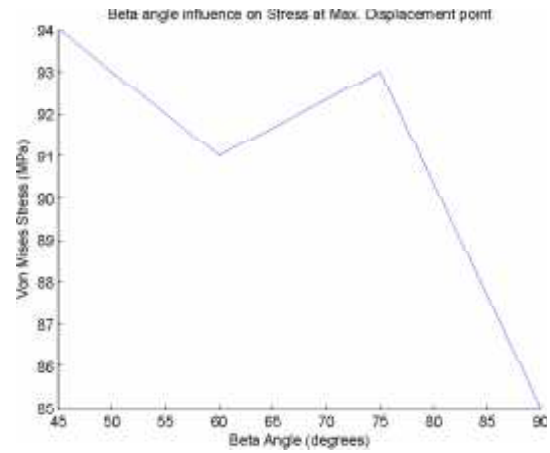
This decision is made because this model presented the lowest stress values and the lowest nodal displacement value. The use of the 60 degree model with the same values of w , h and Rad parameters could be a good possibility to manufacture since it had very similar values as the 90 degree model. The advantage of the 60 degree model is that it is easier to manufacture.

The maximum displacement from this particular model was 0.299 mm. When comparing it from the unmodified model, there is a difference of 0.381 mm, and an improvement of 66%. The maximum Von Mises Stress value is 123 MPa. Comparing it from the unmodified model, there is an improvement of 34%. The stress at the maximum displacement point is 57 MPa. This place had the highest improvement, with a 66% change.

In figure 53 the stress distribution is shown. Different from section 6.5, the stress distribution is not very even. This could indicate that the “snake algorithm” is dependant from the cross section. In other words, the bead pattern and the cross section are dependant from each other.

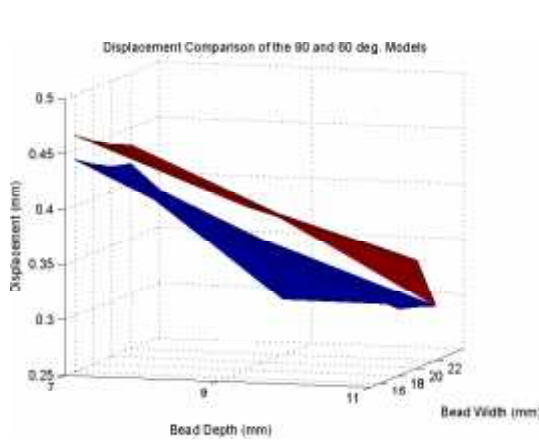


50.1: Influence of β angle against maximum displacement

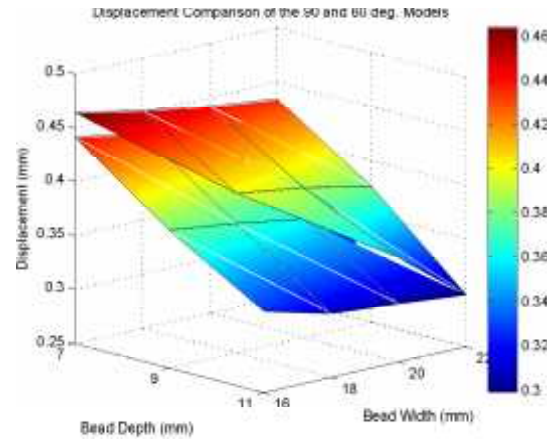


50.2: Influence of β angle against stress variation

Figure 50: Influence of the β angle.



51.1: Displacement comparison of 60 (red) and 90 (blue) degrees models (lateral view)



51.2: Displacement comparison of 60 and 90 degrees models (isometric view)

Figure 51: Two views comparing the nodal displacement between the 60 and 90 degrees models

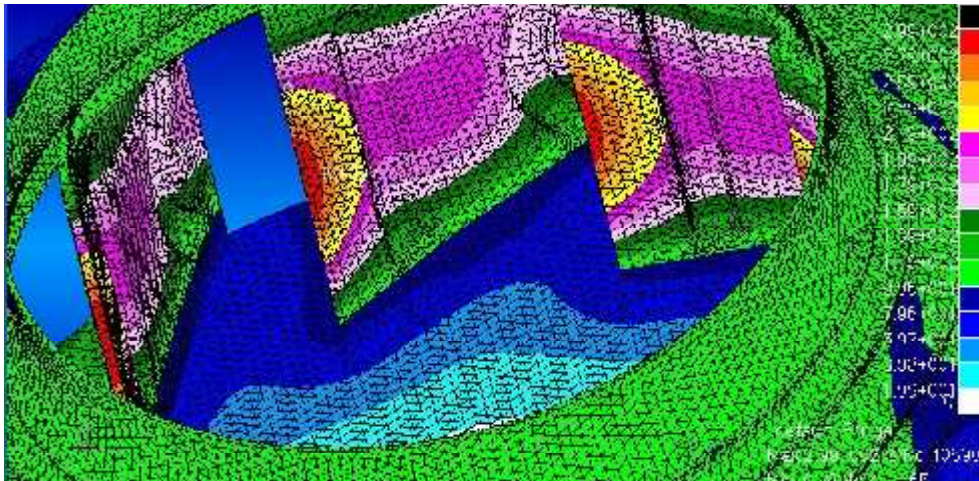


Figure 52: Displacement distribution colormap.

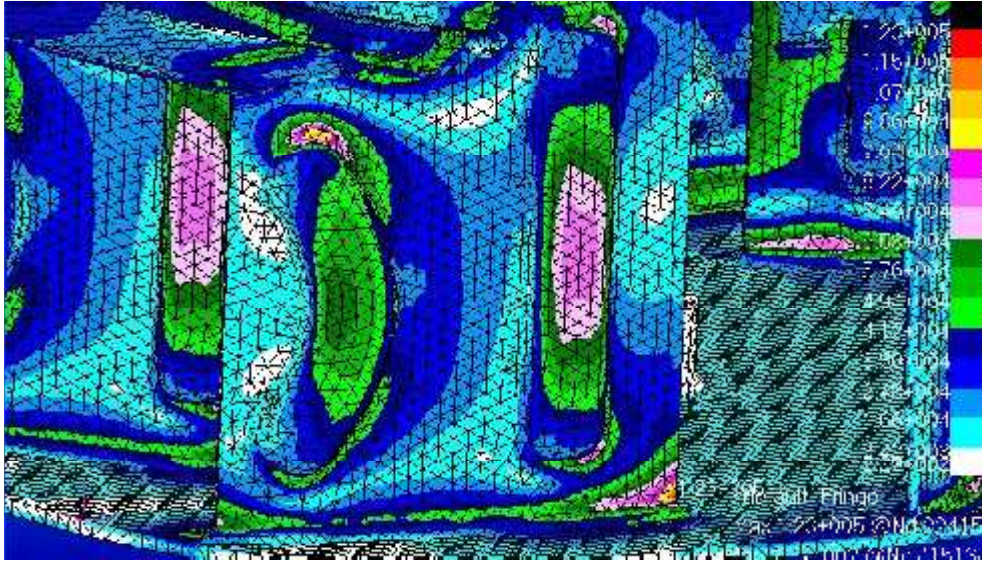
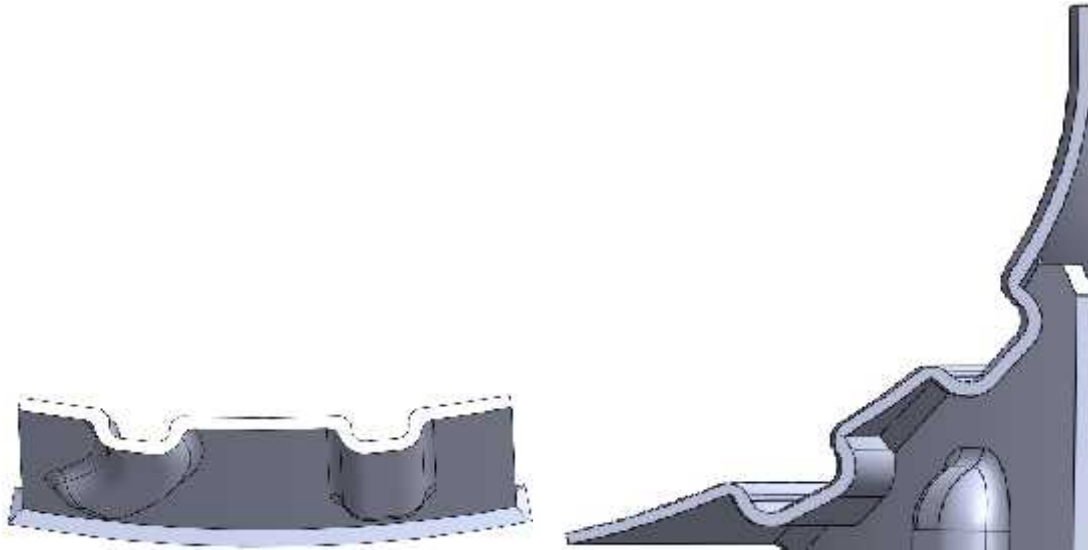


Figure 53: Von Mises stress distribution colormap.



54.1: Final cross section of the blade.

54.2: Final cross section of the top ring.

Figure 54: Two renders of the cross sections of the optimized beads.

References

- [1] Bruno Eck. *Ventilatoren: Entwurf und Betrieb der Radial-, Axial- und Querstromventilatoren*. Klassiker der Technik. Springer, Berlin [u.a.], 6. aufl. edition, 2003. XV, 576 S. : zahlr. Ill., graph. Darst.
- [2] Frank P. Bleir. *Fan Handbook: selection, application and design*. McGraw-Hill Professional, New York, first edition, 1997.
- [3] Dieter Emmrich. *Entwicklung einer FEM-basierten Methode zur Gestaltung von Sicken fuer biegebeanspruchte Leitstuetzstrukturen im Konstruktionsprozess = Development of a FEM-based method for the design of bead patterns for channel and support structures under bending load in the design process*. PhD thesis, Karlsruhe, 2005.
- [4] Bernd Klein. *Leichtbau-Konstruktion: Berechnungsgrundlagen und Gestaltung ; mit Tabellen sowie umfangreichen uebungsaufgaben zu allen Kapiteln des Lehrbuchs*. Maschinenelemente und Konstruktion. Vieweg+Teubner Verlag / GWV Fachverlage GmbH, Wiesbaden, Wiesbaden, 8., ueberarbeitete und erweiterte auflage edition, 2009. Online-Ressource : v.: digital.
- [5] Dominik Schwarz. *Gestaltung optimierter Sickenbilder fuer flaechige Strukturen unter Einsatz numerischer Optimierungsverfahren*. PhD thesis, Aachen, 2003. ; Gb. : EUR 25.00.
- [6] S.N. Patnaik and D.A. Hopkins. Optimality of a fully stressed design. *Computer Methods in Applied Mechanics and Engineering*, 165(1-4):215–221, 1998.
- [7] Dominik Schwarz. *Auslegung von Blechen mit Sicken (Sickenatlas)*. FAT-Schriftenreihe ; 168. Forschungsvereinigung Automobiltechnik e.V. (FAT) [u.a.], Frankfurt/M., 2002.
- [8] Gerhard Oehler. *Gestaltung gezogener Blechteile*. Konstruktionsbuecher ; 11. Springer, Berlin [u.a.], 1951.
- [9] O. Kienzle. Die versteifung ebener boeden und waende aus blech. *Mitteilungen der Forschungsgesellschaft Blechverarbeitung*, 6(7):77–83, 1955.
- [10] G Oehler and E Draeger. Versteifen von stahlbechteilen. *Merkblatt Stahl*, 350, 1971.
- [11] Anton Oehler, Gerhard ; Weber. *Steife Blech- und Kunststoffkonstruktionen*. Konstruktionsbuecher ; 30. Springer, Berlin, 1972.
- [12] Michael Widmann. *Herstellung und Versteifungswirkung von geschlossenen Halbrundsicken*. PhD thesis, Berlin, 1984.
- [13] B Klein. Praxisfaehiges werkzeug zur kontouroptimierung. *Technica Zuerich*, 44(22), 1995.

- [14] Frank Herrmann. *Rechnerische Untersuchung von ausgesteiften Karosserieblechen hinsichtlich ihres Steifigkeitsverhaltens und der auftretenden Spannungskonzentrationen unter Last*. PhD thesis, Aachen, 1997. ; kart.
- [15] B. Krnauer, N. Majic, H. Hoffmann, and A. Albers. Influence of production constraints on automatic generation of bead design. *International Journal of Material Forming*, 3:109–112, 2010. 10.1007/s12289-010-0719-y.
- [16] Lieven Vandenbergh. *Convex optimization*. Cambridge Univ. Press, Cambridge [u.a.], reprinted edition, 2007. XIII, 716 S. : graph. Darst.
- [17] Peter R. Nelson, Marie Coffin, and Karen A. F. Copeland. *Introductory statistics for engineering experimentation*. Elsevier, Amsterdam [u.a.], 2003. XII, 514 S.
- [18] Timothy W. Simpson, Jesse D. Peplinski, Patrick N. Koch, and Janet K. Allen. On the use of statistics in design and the implications for deterministic computer experiments. In *Proceedings of DETC97*. ASME, 1997.
- [19] Kurt Lange. *Umformtechnik : Handbuch fr Industrie und Wissenschaft: Blechbearbeitung*, volume 3. Springer, Berlin [u.a.], second edition edition, 1990.
- [20] Madlen. Baumert, Jokisch. Sebastian, and Heide. von Seggern. Untersuchung der auswirkung von unterschiedlichen sickenformen auf die resultierenden spannungen und verformungen eines rotierenden verdichterrades. 2009.
- [21] C. Koukouvinos. An algorithmic construction of four level response surface designs. *Communications in Statistics: Simulation and Computation*, 38:2152–2160, 2009.
- [22] Ralf Woll and Carina Burkhard. Full factorial design, taguchi design or genetic algorithms teaching different approaches to design of experiments. In Daniel Baier and Klaus-Dieter Wernecke, editors, *Innovations in Classification, Data Science, and Information Systems*, Studies in Classification, Data Analysis, and Knowledge Organization, pages 567–574. Springer Berlin Heidelberg, 2005.
- [23] James Barrett. The coefficient of determination-some limitations. *The American Statistician*, 28:19–20, 1974.
- [24] Dominik Schwarz. *Gestaltung optimierter Sickenbilder fr flchige Strukturen*, volume 6403. Schriftenreihe Automobiltechnik, Aachen, first edition, 2003.
- [25] Bernd Klein. *Leichtbau-Konstruktion: Berechnungsgrundlagen und Gestaltung ; mit 58 Tabellen und umfangreichen bungsaufgaben zu allen Kapiteln des Lehrbuchs*. Viewegs Fachbcher der Technik. Vieweg, Braunschweig [u.a.], 5., berarb. aufl edition, 2001. XII, 484 S ; 24 cm : Ill., graph. Darst.

- [26] Harald Kugler. *Umformtechnik: Umformen metallischer Konstruktionswerkstoffe ; mit 20 Tabellen, 273 Fragen sowie einer DVD*. Fachbuchverl. Leipzig im Carl Hanser Verl., Mnchen, 2009. 391 S. ; 25 cm. 1 DVD (12 cm) : Ill., graph. Darst.

Appendices

A Matlab script to run multiple .bdf files in series

```
clear all
close all
clc
tic;
%asking the user for the paths
[filename, pathname, filterindex] = uigetfile({'*.bdf','BDF Patran File'; ...
    '*.dat','Patran File'}, 'MultiSelect', 'on');

if isempty(filename)
    %checking the files selected
    disp('error: No valid or no file selected')
else
    if isstr(filename)
        %if only a single file was selected
        file_to_run=strcat(pathname,filename);
        disp('Running file')
        disp(file_to_run)
        dos(file_to_run);
        pause(5)
        disp('finished')
        disp('')
        disp('')
    else
        %if several files were selected
        for i=1:size(filename,2)
            file_to_run=strcat(pathname,filename{i});
            disp('Running file')
            disp(file_to_run)
            dos(file_to_run);
            pause(5)
            disp('finished')
            disp('')
            disp('')
        end
    end
end
%show the time the simulations took
toc
```